

THE ORIGIN OF DUST EXTINCTION CURVES WITH OR WITHOUT THE 2175 Å BUMP IN GALAXIES: THE CASE OF THE MAGELLANIC CLOUDS

KENJI BEKKI

ICRAR, M468, The University of Western Australia 35 Stirling Highway, Crawley Western Australia, 6009, Australia

HIROYUKI HIRASHITA

Institute of Astronomy, and Astrophysics, Academia Sinica, PO Box 23-141, Taipei 10617, Taiwan

AND

TAKUJI TSUJIMOTO

National Astronomical Observatory, Mitaka-shi, Tokyo 181-8588, Japan

Draft version April 18, 2018

ABSTRACT

The Large and Small Magellanic Clouds (LMC and SMC, respectively) are observed to have characteristic dust extinction curves that are quite different from those of the Galaxy (e.g., strength of the 2175 Å bump). Although the dust composition and size distribution of the Magellanic Clouds (MCs) that can self-consistently explain their observed extinction curves have been already proposed, it remains unclear whether and how the required dust properties can be achieved in the formation histories of the MCs. We therefore investigate the time evolution of the dust properties of the MCs and thereby derive their extinction curves using one-zone chemical evolution models with formation and evolution of small and large silicate and carbonaceous dust grains and dusty winds associated with starburst events. We find that the observed SMC extinction curve without a conspicuous 2175 Å bump can be reproduced well by our SMC model, if the small carbon grains can be selectively lost through the dust wind during the latest starburst about 0.2 Gyr ago. We also find that the LMC extinction curve with a weak 2175 Å bump can be reproduced by our LMC model with less efficient removal of dust through dust wind. We discuss possible physical reasons for different dust wind efficiencies between silicate and graphite and among galaxies.

Subject headings: Magellanic Clouds – galaxies: evolution – galaxies: ISM – ISM: dust, extinction

1. INTRODUCTION

The Large and Small Magellanic Clouds (LMC and the SMC respectively), which are the closest pair of interacting dwarf galaxies around the Milky Way (MW), have long served as an ideal laboratory to study many aspects of galaxy formation and evolution, such as significant influences of galaxy interaction on galactic star formation and chemical enrichment histories (e.g., Westerlund 1997). Structures and kinematics (e.g., Cole et al. 2005; Nidever et al. 2012), age and metallicity distributions of stellar populations (e.g., Da Costa & Hatzidimitriou 1998; Piatti et al. 2001; Carrera et al. 2008), proper motions (e.g., Kallivayalil et al. 2006; Cioni et al. 2014), and gas and dust contents (e.g., Kim et al. 1999; Meixner et al. 2011; Galliano et al. 2011) have been extensively investigated so far. These observed physical properties of the Magellanic Clouds (MCs) have been used to constrain theoretical models for the MC evolution, such as the 3D orbits around the MW and the LMC-SMC interaction histories and their influences on the star formation histories (e.g., Gardiner & Noguchi 1995; Diaz & Bekki 2011).

One of the long-standing problems related to the physical properties of the MCs is the origin of their extinction curves that are quite different from those of the MW (e.g., Fitzpatrick 1989). The MW extinction curve clearly shows the 2175 Å feature (“bump”) whereas the 2175 Å bump is almost absent in the SMC and rather weak in

the LMC (e.g., Savage & Mathis 1979; Rocca-Volmerange et al. 1981; Prevot et al. 1984; Clayton & Martin 1985; Fitzpatrick 1985; Gordon & Clayton 1998; Gordon et al. 2003). Furthermore, the extinction curves of the MCs at shorter wavelengths ($1/\lambda > 5\mu\text{m}^{-1}$) are different from those of the MW in the sense that they more steeply rise (e.g., Hutchings 1982; Nandy et al. 1982; Bromage & Nandy 1983). These observations suggest that the optical and physical properties of dust grains (e.g., size distributions) in the MCs are quite different from those of the MW for some physical reason.

Pei (1992) adopted the graphite-silicate grain model for the MCs and demonstrated that the observed extinction curves can be reproduced reasonably well by the models with different abundance ratios of graphite to silicate. Weigartmer & Draine (2001) successfully reproduced the observed extinction curves of the MCs and the MW by adopting a simple functional form for the size distributions of carbonaceous and silicate grains. Although these previous studies clarified dust compositions and size distributions required for explaining the observed extinction curves of the MCs, it remains unclear whether and how the required dust properties can be achieved in the formation histories of the MCs. Since the time evolution of dust properties depends on star formation and chemical enrichment histories of galaxies (e.g., Dwek 1998), a dust evolution model that can explain self-consistently the observed SFH and chemical abundances of the MCs needs to

be constructed for better understanding the origin of the extinction curves of the MCs.

Asano et al. (2013) have first incorporated the time evolution of dust size distributions into one-zone chemical evolution models in a fully self-consistent manner and thereby discussed what determines the dust size evolution in galaxies. Nozawa et al. (2015) have additionally incorporated the molecular cloud phase hosting quick dust growth and thereby shown that the observed peculiar extinction curves of high-redshift quasars ($z \geq 4$) can be reproduced, if the quasars can have both a rather high molecular gas fraction (≥ 0.5) and amorphous carbon instead of graphite. These studies, however, have not attempted to reproduce the observed characteristic extinction curves with the nearly absent 2175 Å feature in the SMC and the weak one in the LMC. Although recent numerical simulations of the MCs have shown the time evolution and the spatial distributions of dust abundances in the MCs (Yozin & Bekki 2014), they did not show the size distribution of dust grains in the MCs. Thus, it remains theoretically unclear in what physical conditions the observed extinction curves of the MCs can be reproduced in the evolution models of the MCs.

The purpose of this paper is to investigate the dust extinction curves of the MCs by using new one-zone chemical evolution models with the evolution of dust abundances, compositions, and size distributions. In particular, we investigate in what physical conditions the observed characteristic extinction curves can be reproduced in the new models. Since star formation histories (SFHs), age-metallicity relations (AMRs), and chemical properties (e.g., [Fe/H] and [α /Fe]) of the MCs have been derived (e.g., Harris & Zaritsky 2009; Rubele et al. 2012), we need to construct chemical evolution models that are consistent with these observations. Furthermore, recent observational studies by infrared space telescopes, Akari, Spitzer, and Herschel, have revealed a number of intriguing dust properties in the MCs (e.g., Meixner et al. 2010). These observations can be used to constrain the present dust evolution models for the MCs (e.g., Galliano et al. 2011).

The plan of the paper is as follows: In the next section, we describe our new one-zone chemical evolution models which include not only some key dust-related physical processes (e.g., growth and destruction) but also radiation-driven dust wind depending on dust grains. In §3, we present the results on the time evolution of the extinction curves for the representative SMC, LMC, and MW models. In §4, we discuss (i) the validity of the present new scenario that explains the origin of the observed extinction curves of the MCs and (ii) alternative ones. We do not discuss the details of the chemical evolution of the SMC and the LMC and their dependences on the evolution histories of the MCs in the present paper, because they have been already discussed in our previous papers (e.g., Tsujimoto & Bekki 2009; Bekki & Tsujimoto 2010, 2012, BT12).

Although the formation process of dust in supernovae (SNe) and Asymptotic Giant Branch (AGB) stars in the MCs have been investigated both observationally and theoretically (e.g., Matsuura et al. 2011; Zhukovska & Henning 2013; Schneider et al. 2014), we do not discuss these issues in the present paper. The observed spatial distri-

butions of dust properties in the MCs (e.g., Galliano et al. 2011) are not discussed either in the present study, because they are beyond the scope of this paper. The present one-zone models do not allow us to investigate the observed spatial variations in the extinction curves of the MCs (e.g., Gordon & Clayton 1998), and we will discuss this important issue in our future papers in which hydrodynamical simulations of the MCs with a model for dust size distributions will allow for such an investigation of the spatial variation of the extinction curves.

2. THE MODEL

2.1. Outline

We adopt the following two steps to derive the dust extinction curves of the MCs. First, we investigate the time evolution of dust grains by using one-zone chemical evolution models of the MCs that have been developed by BT12. Second, we derive the extinction curves based on the abundances of dust grains by using the “two-size approximation model” developed by Hirashita (2015; H15). In this two-size approximation, the whole grain population is represented by small grains (radius a less than $0.03 \mu\text{m}$) and large grains ($a > 0.03 \mu\text{m}$), because the major grain processing mechanisms work differently on small and large grains (H15). The original purpose of this two-size approximation method is to use it in statistical (theoretical) predictions and Nbody+hydrodynamical simulations of galaxy formation and evolution and thereby to dramatically reduce the total amount of calculation time for estimating the dust extinction curve for each galaxy and each particle of a simulated galaxy. We use the method in the present study, because we need to run numerous models and the method enables us to complete such calculations of extinction curves much faster.

In the first step, each element (e.g., C, O, and Si) is divided into gas-phase metals and dust, and dust is further divided into “small” and “large” grains. We accordingly investigate the time evolution of the three components, gas-phase metals and small and large grains, separately for each element (e.g., C, O, and Si) in a model. The time evolution of small and large grains can be used for the derivation of the extinction curve in the second step. As demonstrated by H15, the two-size approximation for a dust size distribution is very useful and convenient, because a full calculation of the dust size distribution in a galaxy is complicated and time-consuming (e.g., Asano et al. 2013). Accordingly we adopt the revised version of the two-size approximation model (H15) in order to derive the extinction curve of a galaxy in the second step. In the revised version of the two-size approximation model, the dust in the ISM of a galaxy is divided into four grains; small and large silicate (referred to as small and large “Si-grains”, respectively) and small and large carbonaceous grains (small and large “C-grains”, respectively). This two-size, two-component dust grain model enables us to derive the extinction curve of a galaxy based on the chemical evolution of the galaxy, as described later.

Star formation histories (SFHs) of galaxies can control their chemical evolution histories, because chemical evolution depends on the time evolution of metals ejected from SNe and AGB stars, the formation rates of which depend on star formation rates (SFRs). Therefore, the dust evo-

lution histories of galaxies, which depend on their chemical evolution histories, can be controlled by their SFHs. Since we mainly discuss the extinction curves of the MCs, we need to choose carefully the model parameters for star formation of the MCs. Many observations suggest that the MCs have experienced at least a few starburst (SB) events in the past 6 Gyrs (e.g., Harris & Zaritsky 2004, 2009; Rubele et al. 2012, 2015). Furthermore, previous and recent numerical simulations of the MCs have demonstrated that highly enhanced star formation is inevitable during the past LMC-SMC-Galaxy tidal interaction (e.g., Yoshizawa & Noguchi 2003; Bekki & Chiba 2005; Yozin & Bekki 2014). We consider these observational and theoretical results in constructing the SFHs of the MCs.

Since the importance and possibility of dust removal from galaxies through energetic radiation-driven dust wind in one-zone chemical evolution models have been discussed extensively by Bekki & Tsujimoto (2014, BT14), we do not discuss this issue in detail in this paper. The present model is more sophisticated than BT14 in the sense that it investigates the evolution of gas-phase metals and the formation and evolution of different dust grains in a self-consistent manner. Furthermore, the present model newly includes, the accretion of gas-phase metals onto already existing dust grains, its dependence on cold gas fraction in the ISM, grain growth by coagulation, and grain disruption by shattering. Thanks to this, we can provide more reliable predictions on the time evolution of dust grains in a galaxy.

2.2. Basic equations

We adopt a revised version of our one-zone chemical evolution models used in BT12 in order to investigate the time evolution of gas, metals, and dust in a fully self-consistent manner. Although there are only two basic equations in BT12, there are four in the present study, which reflects the fact that the revised version includes the evolution of small and large dust grains. We investigate the time evolution of the total masses of gas (M_g) and that of the total masses of metal (M_z) and dust (M_d) for each element (e.g., C and O) in a model. Since the total metal mass includes gas-phase metals and dust, the total mass of *gas-phase metals* that is not depleted onto dust grains ($M_{z,g}$) can be estimated as $M_z - M_d$ in the present study. The total gas mass ($M_{g,t}$) accreted onto a galaxy is set to be 1.0 (i.e., normalized) in all models of the present study. The basic equations for the time evolution of gas and metals in the adopted one-zone chemical evolution models with dust physics are described as follows:

$$\begin{aligned} \frac{dM_g}{dt} &= -\alpha_1\psi(t) + A(t) - w(t) - w_d(t) \quad (1) \\ \frac{dM_{z,i}}{dt} &= -\alpha_1 Z_i(t)\psi(t) + Z_{A,i}(t)A(t) + y_{\text{II},i}\psi(t) \\ &\quad + y_{\text{Ia},i} \int_0^t \psi(t-t_{\text{Ia}})g(t_{\text{Ia}})dt_{\text{Ia}} \\ &\quad + \int_0^t y_{\text{agb},i}(m_{\text{agb}})\psi(t-t_{\text{agb}})h(t_{\text{agb}})dt_{\text{agb}} \\ &\quad - W_i(t) - W_{d,i}(t) \quad , \quad (2) \end{aligned}$$

where α_1 is the mass fraction locked up in dead stellar remnants and long-lived stars, $\psi(t)$ is the SFR, Z_i is the

metallicity for i th element, $y_{\text{II},i}$, $y_{\text{Ia},i}$, and $y_{\text{agb},i}$ are the chemical yields for the i th element from type II supernovae (SNe II), from Type Ia supernovae (SNe Ia), and from AGB stars, respectively, $Z_{A,i}$ is the abundance of heavy elements contained in the infalling gas, and W_i is the wind rate for each element. The quantities t_{Ia} and t_{agb} represent the time delay between star formation and SN Ia explosion and that between star formation and the onset of AGB phase, respectively. The terms $g(t_{\text{Ia}})$ and h_{agb} are the distribution functions of SNe Ia and AGB stars, respectively, and the details of which are described later in this section. The term h_{agb} controls how much AGB ejecta can be returned into the ISM per unit mass for a given time in equation (2). The total gas masses ejected from AGB stars depend on the original masses of the AGB stars (e.g., Weidemann 2000). Therefore, this term h_{agb} depends on the adopted IMF and the relation between the mass and the lifetime in stars (later described). The term $W_{d,i}$ is the dust wind rate for each element (i.e., w_d is the sum of $W_{d,i}$ for all elements).

The basic equations for the time evolution of the total masses of small ($M_{d,s}$) and large ($M_{d,l}$) grains in the models are described as follows:

$$\begin{aligned} \frac{dM_{d,s,i}}{dt} &= -\alpha_1 D_{s,i}\psi(t) + D_{s,i}(0)A(t) - \frac{M_{d,s,i}}{\tau_{\text{SN},s,i}} \\ &\quad + \frac{M_{d,l,i}}{\tau_{\text{sh},i}} - \frac{M_{d,s,i}}{\tau_{\text{co},i}} + \frac{M_{d,s,i}}{\tau_{\text{acc},s,i}} - W_{d,s,i}(t) \quad (3) \end{aligned}$$

$$\begin{aligned} \frac{dM_{d,l,i}}{dt} &= -\alpha_1 D_{l,i}\psi(t) + D_{l,i}(0)A(t) + f_{c,i}E_{z,i} \\ &\quad - \frac{M_{d,l,i}}{\tau_{\text{SN},l,i}} - \frac{M_{d,l,i}}{\tau_{\text{sh},i}} + \frac{M_{d,s,i}}{\tau_{\text{co},i}} + \frac{M_{d,l,i}}{\tau_{\text{acc},l,i}} - W_{d,l,i}(t) \quad (4) \end{aligned}$$

where $M_{d,s,i}$ and $M_{d,l,i}$ are the masses of small and large grains for i -th element, respectively, $D_{s,i}$ and $D_{l,i}$ are the dust-to-gas-ratios for small and large grains, respectively, $D_{s,i}(0)$ and $D_{l,i}(0)$ are the initial dust-to-gas-ratios for small and large grains (in infalling gas), respectively, $f_{c,i}$ and $E_{z,i}$ are the condensation efficiency of dust and the ejection rate of a metal element, respectively, $\tau_{\text{SN},s,i}$ and $\tau_{\text{SN},l,i}$ are the timescales of dust destruction by SNe for small and large grains, respectively, $\tau_{\text{sh},i}$ is the timescale for shattering of large grains, $\tau_{\text{co},i}$ is the timescale for coagulation of small grains, and $W_{d,s,i}$ and $W_{d,l,i}$ are the dust wind rates for small and large grains, respectively. The dust wind term $W_{d,i}$ in equation (2) is therefore equivalent to $W_{d,s,i} + W_{d,l,i}$.

The ejection rate of metals from SNe and AGB stars ($E_{z,i}$) is described as follows:

$$\begin{aligned} E_{z,i} &= y_{\text{II},i}\psi(t) + y_{\text{Ia},i} \int_0^t \psi(t-t_{\text{Ia}})g(t_{\text{Ia}})dt_{\text{Ia}} \\ &\quad + \int_0^t y_{\text{agb},i}(m_{\text{agb}})\psi(t-t_{\text{agb}})h(t_{\text{agb}})dt_{\text{agb}}. \quad (5) \end{aligned}$$

The formation rate of dust grains from SNe and AGB ejecta at each time step is estimated from $E_{z,i}$ and $f_{c,i}$. It is assumed here that the dust produced by stars is in the large-grain regime (H15). It should be also stressed that the dust condensation efficiency for each i th element is different between SN Ia, SNI, and AGB ejecta and this difference is properly included in the present one-zone models: the way to describe the dust production term in equation (4) is not very accurate, and such description is

adopted only for convenience. In the implementation of the dust production process, the dust production term is calculated in our code as follows:

$$f_{c,i}E_{z,i} = f_{c,\text{SNIa},i}E_{z,\text{SNIa},i} + f_{c,\text{SNII},i}E_{z,\text{SNII},i} + f_{c,\text{AGB},i}E_{z,\text{AGB},i}, \quad (6)$$

where $f_{c,\text{SNIa},i}$, $f_{c,\text{SNII},i}$ and $f_{c,\text{AGB},i}$ are the dust condensation efficiencies for i th element and $E_{z,\text{SNIa},i}$, $E_{z,\text{SNII},i}$ and $E_{z,\text{AGB},i}$ are the metal ejection rates for i th element.

It should be noted here that the way to describe the evolution of gas, metals, and dust in the above equations is slightly different from those adopted in BT12 and H15. For example, we investigate M_g and M_z instead of the gas mass fraction (f_g in BT12) and metallicity (Z_i) in the present study. Also, the timescales for dust accretion, coagulation, and shattering are defined for each element in the present study: they are assumed to be constant for all elements in H15. The dust wind for small and large grains is separately considered, for the first time, in the present study. The details of the models for star formation, chemical evolution, and dust physics in the ISM and the model parameters are described in the following subsections.

2.3. Star formation and gas accretion

The star formation rate $\psi(t)$ is assumed to be proportional to the gas mass with a constant star formation coefficient and thus is described as follows:

$$\psi(t) = C_{\text{sf}}M_g(t). \quad (7)$$

The normalization factor C_{sf} is chosen appropriately so that the final gas mass fraction (and metallicity) can be consistent with the observed one. We assume that C_{sf} is different between (i) the ‘‘quiescent phase’’, when a galaxy shows an almost steady star formation, and (ii) the ‘‘star burst (SB) phase’’, when the galaxy experiences a bursty star formation. Many observational studies showed that the LMC and the SMC have experienced a few SB events in the past 6 Gyr (e.g., Harris & Zaritsky 2006, 2009; Rubele et al. 2012). Guided by these observations, we investigate models in which a starburst can occur three times (‘‘SB models’’), and the first, second, third starbursts are denoted as SB1, SB2, and SB3, respectively. The star formation rate is assumed to be constantly higher for $t_{\text{sb1},s} \leq t \leq t_{\text{sb1},e}$ in SB1, $t_{\text{sb2},s} \leq t \leq t_{\text{sb2},e}$ in SB2, and $t_{\text{sb3},s} \leq t \leq t_{\text{sb3},e}$ in SB3. The star formation coefficient (C_{sf}) is thus described as follows:

$$C_{\text{sf}} = \begin{cases} C_q & \text{for quiescent phase} \\ C_{\text{sb1}} & \text{for SB1} \\ C_{\text{sb2}} & \text{for SB2} \\ C_{\text{sb3}} & \text{for SB3} \end{cases} \quad (8)$$

In the present study, C_{sf} is given for each model (e.g., SMC, LMC, and MW).

We adopt the following formula for the rate of gas accretion onto the disk of a galaxy:

$$A(t) = C_a \exp(-t/t_a), \quad (9)$$

where t_a is a free parameter controlling the timescale of the gas accretion and C_a is the normalization factor and determined such that the total gas mass ($M_{g,t}$) accreted onto the galaxy can be 1 for a given t_a . This $M_{g,t}$ is determined such that $M_{g,t}$ is the total baryonic mass of a (present)

galaxy (i.e., gas and stars, *including gas, metals, and dust ejected from the galaxy through outflow*). The parameter t_a can therefore control the time evolution of the total gas mass and the gas mass fraction of a galaxy. We mainly show the results of the models with $t_a = 5$ Gyr, though we investigated models with different t_a . The main purpose is to discuss how dust wind plays key roles in the evolution of extinction curves of galaxies in the present study. Such roles of dust wind do not depend on the adopted t_a .

Although we show only the results of the models with $t_a = 5$ Gyr, the final (i.e., present) gas masses and gas mass fractions of the three galaxies are roughly consistent with the observed values. For example, if we adopt $M_g = 3 \times 10^9 M_\odot$ (BT12) for the LMC, then the final gas mass is $1.1 \times 10^9 M_\odot$ and the gas fraction is 0.37. These numbers are roughly consistent with the observed values (e.g., van den Bergh 2000), which suggests that the adopted t_a is reasonable. Furthermore the typical star formation rate at non-starburst phases in the LMC models is $0.15 M_\odot \text{ yr}^{-1}$, which is similar to the observed present SFR of the LMC ($0.26 M_\odot \text{ yr}^{-1}$; Kennicutt et al. 1995). The final gas mass fractions of the SMC and the MW are 0.53 and 0.05 in the present models, respectively, which are also roughly consistent with the observed values (e.g., van den Bergh 2000). The evolution of SFRs and gas mass fractions are given in Figure 1 and later discussed.

The assumption of slow gas accretion onto the SMC implies that the SMC has a disk component. Almost all previous theoretical models of the Magellanic Stream (MS) formation needed to assume the gas and stellar disks (e.g., Gardiner & Noguchi 1995; Diaz & Bekki 2012) in order to reproduce quite well the observed properties of the MS. Furthermore, recent observations have confirmed that the SMC has a stellar disk (e.g., Dobbie et al. 2014), and it is a well known fact that the SMC has a rotating HI disk (e.g., Stanimirovic et al. 2004). Therefore, it is reasonable for the present study to assume that the SMC has a disk onto which gas can be accreted.

2.4. SN-driven wind

We assume that some fractions of metals from SNe can be removed from a galaxy thorough energetic outflows so that they do not contribute to chemical enrichment of the galaxy. In the present study only SNe ejecta can be expelled from a galaxy (‘‘selective wind model’’). We do not consider that the ejection efficiency depends on (i) chemical elements (e.g., C and O) and (ii) whether the ejecta is from SN Ia or SN II just for simplicity in the present study. Some fraction, $1 - f_{\text{ej}}$, of gaseous ejecta from SNe can be mixed with the ISM for chemical enrichment processes whereas all AGB ejecta can be mixed with the ISM in the selective wind models.

The SN wind rate ($w(t)$) is estimated only from the total mass of gaseous ejecta from SNe ($M_{\text{ej,sn}}$) at each time step. The total mass, M_w , of ISM that is removed from a galaxy at each time step is as follows:

$$M_w = f_{\text{ej}}M_{\text{ej,sn}}. \quad (10)$$

Therefore, the SN wind rate at each time step is simply

$$w(t) = \frac{dM_w}{dt}. \quad (11)$$

We show the results of the models with $f_{\text{ej}} = 0.4$ in the present study, because BT12 have already investigated the

SN wind models with $f_{\text{ej}} = 0.2$ and 0.4 and confirmed that such models can better reproduce the observed properties of chemical abundances of the LMC (e.g., Figure 16 of BT12). We also confirm that the roles of dust wind in the evolution of extinction curves do not depend strongly on f_{ej} , though the models with lower f_{ej} end up with higher gaseous metallicities.

Multiple SN events can strongly influence the chemical and dynamical evolution of star-forming regions, and one of the most dramatic influences is the formation of super shells and bubbles in the H I disks of the LMC and the SMC (e.g., Kim et al. 1999; Stanimirovic et al. 1999). Such SN events can cause more efficient dust destruction, shattering, and coagulation in shells and bubbles of MCs, which implies that the models of dust evolution would need to include such dust-related physical processes depending on the time evolution of SN rates. In the present study, we do not intend to model such dust-related physical processes dependent on SN rates, mainly because such complicated models require a few additional model parameters and thus would possibly prevent us from clarifying the key parameters for the evolution of dust extinction curves. Thus it would be our future study to include the dust-related physical processes dependent on SN rates of galaxies in dust evolution models.

2.5. Delay time distribution of SN Ia

We assume that there is a time delay (t_{Ia}) between the star formation and the metal ejection from SNe Ia. We here adopt the following delay time distribution, “DTD”, ($g(t_{\text{Ia}})$) for $0.1 \text{ Gyr} \leq t_{\text{Ia}} \leq 10 \text{ Gyr}$, which is deduced from recent observational studies on the SN Ia rate in extragalaxies (e.g., Maoz et al. 2010);

$$g_{\text{Ia}}(t_{\text{Ia}}) = C_{\text{g}} t_{\text{Ia}}^{-1}, \quad (12)$$

where C_{g} is a normalization constant that is determined by the number of SN Ia per unit mass (which is controlled by the IMF and the binary fraction for intermediate-mass stars for the adopted power-law slope of -1). We mainly investigate models with the above DTD (rather than those with typical time delay of SN Ia being $\sim 1 \text{ Gyr}$). The fraction of the stars that eventually produce SNe Ia for $3\text{--}8M_{\odot}$ has not been observationally determined and thus is regarded as a free parameter, f_{b} . We investigate models with $f_{\text{b}} = 0.05$, because such models can better explain the observed chemical properties of the MCs and the Galaxy (e.g., Tsujimoto et al. 2010; BT12).

2.6. Nucleosynthesis and dust yields

We adopt the nucleosynthesis yields of SNe II and Ia from T95 to deduce $y_{\text{II},i}$ and $y_{\text{Ia},i}$ for a given IMF. For AGB yields, we calculate $y_{\text{agb},i}$ and $h(t_{\text{agb}})$ for a given IMF based on the yield tables from van den Hoek & Groenewegen (1997). Since our recent chemodynamical simulations of disk galaxy formation can reproduce the basic dust properties of galaxies (e.g., dust-to-gas-ratios) reasonably well (Bekki 2013), we adopt the dust yields (corresponding to $f_{\text{c},i}$) used in the simulations for the present study. The adopted $f_{\text{c},i}$ is originally from Dwek (1998), which explained the dust properties of the Galaxy quite well. The adopted values are different between different

elements and between SNe and AGB stars. We investigate the time evolution of dust and metals for the selected eight elements, C, O, Mg, Fe, Ca, Si, Ti, and S.

2.7. IMF

We adopt a standard power-law IMF;

$$\Psi(m_{\text{I}}) = M_{\text{s},0} m_{\text{I}}^{-\alpha}, \quad (13)$$

where m_{I} is the initial mass of each individual star and the slope α is set to be 2.35, which corresponds to the Salpeter IMF (Salpeter 1955). The normalization factor $M_{\text{s},0}$ is a function of α , m_{l} (lower mass cut-off), and m_{u} (upper mass cut-off). These m_{l} and m_{u} are set to be $0.1M_{\odot}$ and $50M_{\odot}$, respectively. As discussed in BT12, the IMF slope α can influence the chemical evolution history of the LMC. We however did not discuss such an influence in the present study, firstly because the purpose of this paper is not to clarify the roles of IMF in galactic chemical evolution and secondly because the models with the standard IMF (with SN wind) can explain the observed abundances of the MCs (e.g., Tsujimoto & Bekki 2009; BT12).

The IMF slope can possibly influence the evolution of dust and metals of galaxies, because it can influence the total amount of energy ejected from massive stars and SNe. If we adopt a top-heavy IMF (e.g., $\alpha = 2.1$ instead of 2.35), then dust and metals can be more efficiently ejected from the MCs so that dust-to-gas-ratios can be lower in the MCs. The time evolution of extinction curves of the MCs might be changed to some extent owing to the more efficient removal of dust. Although this is an important issue, we do not investigate how the IMF can influence the evolution of dust and extinction curves of the MCs in the present study: It is our future study to clarify these IMF influences.

2.8. Two-composition approximation

Although we investigate the time evolution of small and large grains for each element (e.g., C, O, and Mg) *separately*, we divide these grains into the following two categories: C-grains and Si-grains. Dust grains formed from the element C are referred to as C-grains whereas those from elements other than C are referred to as Si-grains. Asano et al. (2013) also adopted this treatment of Si-grains, expecting that solid materials other than carbonaceous dust compose silicate materials after dust processing in the ISM. Accordingly, there are four different types of grains (*four-component dust model*), for each of which the total mass and dust-to-gas-ratio (D) are investigated in the present study. For example, the dust-to-gas-ratio for small Si-grains is estimated as follows:

$$D_{\text{s,si}} = \sum_i D_{\text{s,i}}, \quad (14)$$

where the summation is done for elements other than C (i.e., only for $i=\text{O, Fe, Mg, Ca, Si, Ti, and S}$). The dust-to-gas-ratio for small C-grains is simply $D_{\text{s,C}}$. Thus, the total dust-to-gas-ratio (D) is given as:

$$D = \sum_i \sum_j D_{i,j}, \quad (15)$$

where summation is done over $i=\text{s}$ (small) and l (large) and $j=\text{C, O, Fe, Mg, Ca, Si, Ti, and S}$.

2.9. Dust growth

We consider (i) that dust grains can grow quite efficiently through the accretion of gas-phase metals onto the grains in the cold molecular clouds, (ii) that the timescale is shorter for clouds with higher metal-abundance, and (iii) that dust accretion timescale ($\tau_{\text{acc},s,i}$ and $\tau_{\text{acc},l,i}$) depends on the metallicity and the molecular gas density in ISM. The accretion timescale for the small grain of i th element is therefore as follows:

$$\tau_{\text{acc},s,i} = \frac{\tau_{\text{acc},s,i,\odot}}{C_{\text{acc},i}}, \quad (16)$$

where $\tau_{\text{acc},s,i,\odot}$ is the dust accretion timescale at the solar metallicity (0.014) and the total dust abundance (0.0064) at the solar neighborhood (in the present MW), and the correction factor $C_{\text{acc},i}$ is as follows:

$$C_{\text{acc},i} = F(Z_{z,g}, f_{\text{H}_2}) = \frac{Z_{z,g}}{Z_{z,g,\odot}} \left(\frac{D}{D_{\odot}} \right)^{\beta}, \quad (17)$$

where D , $Z_{z,g}$, f_{H_2} are the dust-to-gas-ratio, the gas-phase metallicity, and the cold gas (molecular gas) fraction, respectively, and $Z_{z,g,\odot}$ and D_{\odot} are the gas-phase metallicity and the dust-to-gas-ratio at the solar neighborhood, respectively. Here, D_{\odot} is the total dust-to-gas-ratio and thus set to be 0.0064, and β relates the dust-to-gas-ratio to the molecular fraction of ISM. In this formula, we adopt a very reasonable assumption that the dust accretion timescale is shorter in higher metallicity and higher cold gas fraction. The cold gas fraction is assumed to be a function of D as follows:

$$f_{\text{H}_2} \propto \left(\frac{D}{D_{\odot}} \right)^{\beta}, \quad (18)$$

where we estimate f_{H_2} by using D and gas mass at each time step in a model. We choose this β of 0.2 for f_{H_2} , because such a choice is consistent with recent observational results by Corbelli et al. (2012) who show a correlation between the total masses of molecular hydrogen and dust in galaxies.

Although we adopt the exactly the same formula for the dust accretion timescale ($\tau_{\text{acc},l,i}$) of large grains, we consider that $\tau_{\text{acc},l,i,\odot}$ should be significantly longer than $\tau_{\text{acc},s,i,\odot}$ owing to the possible mass growth timescale proportional to dust sizes (H15). We therefore assume that $\tau_{\text{acc},l,i,\odot}$ is $10\tau_{\text{acc},s,i,\odot}$ for all models. We show the results of the models with $\tau_{\text{acc},s,i,\odot} = 0.02$ Gyr $\tau_{\text{acc},l,i,\odot} = 0.2$ Gyr for all elements in the present study. The dust destruction timescale ($\tau_{\text{SN},s,i}$ and $\tau_{\text{SN},l,i}$) is set to be 0.2 Gyr for small and large grains of all elements, and these values are similar to those adopted in previous studies (e.g., Dwek 1998; H15).

2.10. Coagulation and shattering

As discussed by H15, the timescales of coagulation and shattering depend on D (dust-to-gas-ratio) in the ISM of galaxies. We therefore adopt the following formula:

$$\tau_{\text{sh},i} = \tau_{\text{sh},i,\odot} \left(\frac{D_{1,i}}{D_{1,i,\odot}} \right)^{-1}, \quad (19)$$

where $\tau_{\text{sh},i,\odot}$ and $D_{1,i,\odot}$ are $\tau_{\text{sh},i}$ and $D_{1,i}$ (dust-to-gas-ratio for large grains) at the solar neighborhood, respectively. Since C (carbon) becomes carbon dust whereas metals

other than C become silicate, the shattering timescale for large C-grains is as follows:

$$\tau_{\text{sh},i} = \tau_{\text{sh},C,\odot} \left(\frac{D_{1,C}}{D_{1,\odot}} \right)^{-1}, \quad (20)$$

where $D_{1,C}$ is the dust-to-gas-ratio of large C-grains and $D_{1,\odot}$ is the dust-to-gas-ratio for large grains (0.0045) at the solar neighborhood. The timescale for elements other than C is as follows:

$$\tau_{\text{sh},i} = \tau_{\text{sh},\text{Si},\odot} \left(\frac{D_{1,\text{Si}}}{D_{1,\odot}} \right)^{-1}, \quad (21)$$

where $D_{1,\text{Si}}$ is the dust-to-gas-ratio of large Si-grains. We choose $\tau_{\text{sh},C,\odot} = \tau_{\text{sh},\text{Si},\odot} = 0.1$ Gyr, which is similar to those adopted in previous studies (e.g., H15).

Similarly, the coagulation timescale for C is described as follows:

$$\tau_{\text{co},i} = \tau_{\text{co},C,\odot} \left(\frac{D_{s,C}}{D_{s,\odot}} \right)^{-1}, \quad (22)$$

where $D_{1,C}$ is the dust-to-gas-ratio of small C-grains and $D_{1,\odot}$ is the dust-to-gas-ratio for small grains (0.0019) at the solar neighborhood. The coagulation timescale for elements other than C is as follows:

$$\tau_{\text{co},i} = \tau_{\text{co},\text{Si},\odot} \left(\frac{D_{s,\text{Si}}}{D_{s,\odot}} \right)^{-1}, \quad (23)$$

where $D_{1,\text{Si}}$ is the dust-to-gas-ratio of small Si-grains. The values of $\tau_{\text{co},C,\odot}$ and $\tau_{\text{co},\text{Si},\odot}$ are set to be 0.02 Gyr, which is similar to those adopted by other studies (e.g., H15).

2.11. Radiation-driven dust wind

The new model for dust wind rate $W_d(t)$ in the present study is different to some extent from those adopted in our previous study (BT14). The wind rate is assumed to be different not only between C- and Si-grains but also between small and large grains in the new model. Therefore the wind rate $W_d(t)$ is described as follows:

$$W_d(t) = C_w S(t) M_d(t), \quad (24)$$

where C_w is a parameter that controls the removal efficiency of dust through dust wind, $S(t)$ is the total luminosity (proportional to the strength of radiation pressure of stars), and M_d is the total dust mass. The physical meaning of C_w , which is the most important parameter in the present study, is clearly explained and discussed in Appendix A. About 0.4% of dust can be lost through radiation-driven stellar wind within 10^6 yr in a model with $C_w = 0.01$.

The value of C_w can be different between small and large C-grains and Si-grains. For example, the wind rate for small C-grains ($C_{w,s,C}$; $i=C$) is given as:

$$W_{d,s,C}(t) = C_{w,s,C} S(t) M_{d,s,C}, \quad (25)$$

where $C_{w,s,C}$ is the value of C_w for small C-grains. As demonstrated by recent numerical simulations of dust wind in galaxies (Bekki 2015), it depends on a number of factors whether dust can be ejected and removed from galaxies beyond their halo regions. For example, gas-dust interaction through gaseous drag can prevent dust from being ejected from gas disks of galaxies. Since this gas-dust interaction can not be modeled in the present one-zone models, we regard C_w as a free parameter. Thus, we investigate the effects of dust wind in the evolution of dust by changing the C_w parameters for different grains.

In the present study, we assume that dust wind can occur only in strong starburst phases (SB1, SB2, and SB3):

no dust can be removed from a galaxy in the quiescent star-formation. This assumption is quite reasonable and realistic, because dust wind is observed in starburst galaxies like M82 (e.g., Kaneda et al. 2010). The strength of radiation pressure of stars in a galaxy is assumed to be proportional to the total luminosity of the galaxy, and the total luminosity is calculated as follows:

$$S(t) = \int_0^t f_{M/L}^{-1}(t-T)M_{\text{ns}}(T)dT, \quad (26)$$

where $f_{M/L}$ is the mass-to-light ratio (M/L) of a single stellar population (SSP) and $M_{\text{ns}}(T)$ is the total mass of stars formed at $t=T$. Since the M/L of a SSP is a function of age and metallicity, we need to use a stellar population synthesis code in order to properly calculate $f_{M/L}$ at each time step. Accordingly, we use the code MILES (Vazdekis et al. 2010) for the M/L estimation of all models in the present study. We adopt the SSP table for the Salpeter IMF and $[Z/H]=-0.4$ from the MILES and estimate M/L for stars with different ages in all models.

Since the parameter C_w is already introduced in equation (23), the above equation (25) is slightly different from that (with a parameter C_r) used in BT14. The radiation-driven wind can remove dust from a galaxy, and thus C_w is non-zero only for $t_{\text{sb1},s} \leq t \leq t_{\text{sb1},e}$, $t_{\text{sb2},s} \leq t \leq t_{\text{sb2},e}$, and $t_{\text{sb3},s} \leq t \leq t_{\text{sb3},e}$: $C_w = 0$ in the quiescent SF phase. We have run a large number of models with different values of $C_{w,s,C}$, $C_{w,l,C}$, $C_{w,s,Si}$, and $C_{w,l,Si}$ so that we can find models that can explain the observed extinction curves of the LMC and the SMC. We mainly show the results of three “fiducial” models with a particular combinations of these four parameters for the SMC, the LMC, and the MW, because they can reproduce the observed extinction curves.

2.12. Derivation of extinction curves

Based on the total masses (or fractions) of small and large C-grains and Si-grains in a model, we can draw the extinction curve by using the two-size approximation method by H15. Since the details of the method to derive extinction curves from dust masses and compositions are already given in H15, we briefly describe it here. We adopt the “modified” log-normal model for the grain size distribution of small and large grains, and the functional form ($n_{i,j}(a)$) for the distribution is given as follows:

$$n_{i,j}(a) = \frac{C_{i,j}}{a^4} \exp\left\{-\frac{[\ln(a/a_{0,i,j})]^2}{2\sigma^2}\right\}, \quad (27)$$

where a is the grain size, subscript i describes the small ($i=s$) or large ($i=l$) grains, subscript j describes carbonaceous ($j=C$) or silicate ($j=Si$) grains, $C_{i,j}$ is the normalization constant, and $a_{0,i,j}$ and σ are the central grain radius and the standard deviation of the log-normal distribution, respectively. It should be noted here that the mass distribution ($\propto a^3 n_{i,j}(a)$) is log-normal in the adopted model.

We adopt $a_{0,,s,C} = a_{0,,s,Si} = 0.005 \mu\text{m}$, $a_{0,,l,C} = a_{0,,l,Si} = 0.1 \mu\text{m}$, and $\sigma = 0.75$ so that the size distribution function can roughly cover the small and large grain size ranges. The normalizing constant for small and large C-grains and Si-grains are determined by the following equation:

$$\mu_{\text{H}} D_{i,j} = \int_0^\infty \frac{4}{3} \pi a^3 s n_{i,j}(a) da, \quad (28)$$

where $\mu = 1.4$ is the gas mass per hydrogen nucleus, m_{H} is the hydrogen atom mass, and s is the material density of a dust grain. Accordingly, we can derive $C_{i,j}$ for $D_{i,j}$ derived from one-zone chemical evolution models by using the above equation.

Based on $n_{i,j}$ estimated from $D_{i,j}$ at each time step in a chemical evolution model, we can derive the dust extinction curve at the time step. The extinction at wavelength λ in units of magnitude (A_λ) normalized to the column density of hydrogen nuclei (N_{H}) is described as follows (H15):

$$\frac{A_\lambda}{N_{\text{H}}} = 2.5 \log e \sum_i \sum_j \int_0^\infty n_{i,j} \pi a^2 Q_{\text{ext}}(a, \lambda), \quad (29)$$

where $Q_{\text{ext}}(a, \lambda)$ is the extinction efficiency factor. The values of this Q_{ext} factor at each wavelength and for each grain are evaluated by using the Mie theory (Bohren & Huffman 1983) and the same optical constants for silicate and carbonaceous dust in Weingartner & Draine (2001). We adopt $s = 3.5 \text{ g cm}^{-3}$ for small and large Si-grains and $s = 2.24 \text{ g cm}^{-3}$ for small and large C-grains. As shown in H15, this extinction model can reproduce reasonably well the observed MW extinction curve.

2.13. The model parameters for the MCs and the MW

We first investigated many models with different model parameters for dust growth, shattering, and coagulation and found that no models can reproduce the observed extinction curves without the 2175 Å bump (SMC) and the very weak one (LMC). We then considered the effects of dust wind on the evolution of dust extinction curves by incorporating the dust ejection/removal process associated with dust wind into the one-zone models. Hou & Hirashita (2015) have adopted one-zone models without dust wind for deriving dust extinction curves of galaxies and found that the models with a wide range of parameters for dust-related physical processes (e.g., coagulation) can not reproduce the observed extinction curves without the 2175 Å bump. Therefore, it seems that standard chemical evolution models without dust wind can not reproduce the extinction curves of the MCs.

After extensive investigation of models with dust-related physical processes (e.g., selective destruction of C-grains by SNe and dust wind), we could finally find that models with dust wind can reproduce better the observed extinction curves of the MCs. Therefore, we focus on the results of the models with dust wind in the present study. Although it is possible that physical processes other than dust wind can be responsible for the origin of the extinction curves of the MCs, we focus exclusively on the effects of dust wind on the evolution of extinction curves of the MCs.

We consider that the efficient ejection/removal of dust grains from the SMC and the LMC can be the key physical process for the origin of their dust extinction curves. We therefore (i) change the parameters of dust wind and (ii) adopt reasonable values for other model parameters (e.g., for dust growth) so that we can more clearly elucidate the key factor for the presence or absence of the 2175 Å bump. The model parameters for star formation (e.g., burst epoch) and dust-related physical processes (e.g., dust accretion timescale) are summarized in Table 1

and Table 2, respectively, for the MCs and the MW. BT12 have already discussed how the chemical evolution (thus dust evolution) histories of the MCs depend on star formation parameters, and H15 has discussed how the dust evolution of a galaxy depends on the model parameters for dust growth, destruction, shattering and coagulation. Furthermore, we have confirmed that only some models with dust wind can explain the observed extinction curves of the MCs. Therefore, we focus exclusively on how dust wind plays a key role in controlling the extinction curves of the MCs.

In determining the three burst epochs, we consider both recent observational and theoretical results on the star formation and chemical evolution histories of the MCs. Harris & Zaritsky (2004) investigated the ages of stars in the SMC based on UBVI photometry from their Magellanic Clouds Photometric Survey and found significant rises in the mean star formation rate around 0.06, 0.4, and 2.5 Gyr ago. Using gas dynamical simulations of the SMC interacting with the LMC and the MW, Yoshizawa & Noguchi (2003) predicted that the SMC experienced starburst events about 0.2 Gyr and 1.5 Gyr ago. Rubele et al. (2015) have recently detected the starburst populations with ages of 1.5 and 5 Gyr in the deep images of the SMC from the VISTA survey of the Magellanic Clouds in the YJK_s bands. Guided by these observations, we assume that the SMC experienced three enhanced star formation episodes at $t_{\text{sb},1,s} = 8.5, 11.5, \text{ and } 12.85$ Gyr (assuming the current age of 13 Gyr for the LMC).

The LMC also appears to have experienced at least three major epochs of significantly enhanced star formation. Rubele et al. (2012) investigated the AMR of the LMC stellar populations and found that the SFR peak around 2 Gyr ago, though the AMR appears to be different between different local regions. Based on the results of the gas dynamical simulations of the LMC over the past 6 Gyr, Bekki et al. (2004) suggested that a starburst, which can form globular clusters, could have occurred in the LMC about 3 Gyr ago owing to the LMC-SMC-Galaxy tidal interaction. Harris & Zaritsky (2009) found very strong enhancement of mean star formation from 10^8 yr ago to the present in the blue arm, Constellation III, and 30 Doradus region of the LMC. Thus, we assume that the LMC experienced three enhanced star formation at $t_{\text{sb},1,s} = 10.0, 11.5, \text{ and } 12.85$ Gyr (corresponding to 3, 1.5, and 0.15 Gyr ago, respectively).

Table 3 summarizes the model parameters of dust wind in the three galaxies. Although we investigated much more models than those listed in this table, we show only these representative ones, because they grasp some essential ingredients of the dust wind effects on the extinction curves of galaxies. We mainly describe the time evolution of the extinction curve in the fiducial model for the SMC (S1). This fiducial model is chosen, because it can best reproduce the observed extinction curve of the SMC. As a comparative experiment, the model without dust wind (yet with starburst; S2) is investigated for the SMC. These models with and without dust wind enable us to demonstrate more clearly how the dust wind can change the shapes of the extinction curves of the SMC. The models with different $C_{w,s,C}$ (S3, S4, and S5) are investigated so that the importance of ejection/removal of small C-grains

in the evolution of the extinction curve of the SMC can be more clearly described. The models without starbursts (S6–S9) enables us to understand the importance of starburst dust wind in the evolution of the extinction curve.

We show the results of the LMC models with and without dust wind also in order to clarify the physical reasons for the observed weak 2175 Å extinction bump in the LMC. We show the results of the MW model (M1) without starburst (thus without dust wind) only, because there is little observational evidence for recent strong starburst in the MW. This MW model and those for the MCs (S1 and M1) can combine to demonstrate that the present models can explain not only the extinction curve of the MW but also those of the MCs. Figure 1 shows the time evolution of M_g (normalized), f_g (gas mass fraction), and SFR (normalized) for the fiducial SMC, LMC, and MW models.

3. RESULTS

3.1. SMC

Figures 2 and 3 show the time evolution of the extinction curve and the relative fractions of dust grains, respectively, in the standard SMC model (S1) in which the SMC can experience three strong starburst (SB) events. Before the first SB event (SB1), the star formation rate of the SMC can be kept low so that chemical evolution can proceed very slowly ($T < 8.5$ Gyr). In this low-metallicity phase (pre-SB1 phase), stellar dust production dominates the dust content (i.e., yet little dust growth) since the dust abundance is too low for other dust processing mechanisms (in particular, shattering) to work efficiently. As a result of this, the ISM dust of the SMC is dominated by large grains. The SMC thus can show a rather flat extinction curve without the 2175 Å bump in this pre-SB1 phase.

As the gas-phase metallicity becomes higher through more rapid chemical evolution during SB1, the mass fraction of small grains becomes larger owing to the interplay between shattering and accretion ($T = 9.8$ Gyr). The extinction curve can therefore show a slightly steeper rise in the FUV regime and the 2175 Å bump can be appreciably seen at this post-SB1 phase. The extinction curve becomes progressively steeper and the 2175 Å bump become more prominent after the SB1 ($T = 11.5$ Gyr). The fraction of cold gas can become higher at this epoch, because D , which can determine the gas fraction is higher. The fraction of small Si-grains can be as large as that of large Si-grains at this pre-SB2 phase, because the higher metallicity and the higher cold gas fraction combine to allow the more rapid growth of the small grain abundance. These behaviors in the evolution of Si grains are apparently similar to those reported in Asano et al. (2014).

Although the fraction of small Si-grains can be temporarily lower owing to the efficient destruction of dust by SNe during the second starburst phase (SB2), it can start to rise again soon after SB2 ($T = 12.5$ Gyr). The total mass of small Si-grains becomes 1.6 times larger than that of large Si-grains at $T = 12.5$ Gyr so that the mass fraction of small Si-grains can be the largest in the SMC history. Consequently, the extinction curve of the SMC in this model at $T = 12.5$ Gyr shows a very steep rise that is even steeper than the observed SMC extinction curve and thus inconsistent with the observed curve. Although small

C-grains can also suffer a significant loss of their mass owing to the grain destruction by SNe during SB2, their mass can steadily and rapidly increase through the accretion of gas-phase metals after SB2. This increase of small C-grain abundance is responsible for the strong 2175 Å bump in the extinction curve at $T = 12.5$ Gyr.

The fraction of small Si-grains can become smaller owing to their destruction by SNe and ejection from the SMC through radiation-driven dust wind in the third starburst phase (SB3) so that the extinction curve at $T = 12.9$ Gyr can be slightly less steeper than that at $T = 12.5$ Gyr. The dust wind effects are more significant in this SB3, mainly because the total luminosity of stars in the SMC takes its maximum. Although a significant fraction of small C-grains can be removed from the SMC through dust wind, the extinction curve still clearly shows the 2175 Å bump in the early phase of this SB3. The 2175 Å bump can completely disappear only after most of the small C-grains can be removed from the SMC through dust wind at $T = 12.9$ Gyr. The final extinction curve at $T = 13$ Gyr is very similar to the observed one both in the lack of the 2175 Å bump and in the steep linear rise at FUV wavelength. Thus the present standard SMC model with dust wind can reproduce quite well the observed extinction curve.

As clearly shown in Figure 3, the time evolution of C-grains is different between the SMC models with and without dust wind (S1 and S2, respectively) after SB2: the fractions of small and large C-grains and small Si-grains (relative to large Si-grains) are not so different between the two models during and after SB1 and SB2. This suggests that the SMC can not show the extinction curve without the 2175 Å bump until quite recently. This also suggests (i) that star-bursting dwarf galaxies do not necessarily show extinction curves without the 2175 Å bump and (ii) that dust wind needs to be strong enough to remove most (90 percent) of small C-grains in star-bursting dwarfs with no 2175 Å bump in their extinction curves. It is thus highly likely that starburst dwarfs have different strength of the 2175 Å bump.

Figure 4 shows that the final extinction curve in the SMC model with three SB events yet no dust wind has the conspicuous 2175 Å bump. The SMC models with lower dust wind efficiency ($C_{w,s,C}=0.01$ and 0.03 for S4 and S5, respectively) also show the 2175 Å bump and the FUV rise that is less consistent with the observed extinction curve of the SMC. The SMC model with higher dust wind efficiency ($C_{w,s,C}=0.1$, S6) can reproduce the observed extinction curve of the SMC as well as the standard SMC model. These results confirm that the removal of small C-grains from the SMC through dust wind is a viable mechanism for the observed lack of the 2175 Å bump in the extinction curve of the SMC.

The model with no starburst thus no dust wind (S7) shows the conspicuous 2175 Å bump and a steeper FUV rise, which clearly demonstrates that dust wind can significantly influence the shape of the extinction curve of the SMC. As shown in the models S8 and S9, the presence or absence of the 2175 Å bump does not depend on whether SB1 or SB2 occurs in the SMC. However, the 2175 Å bump of the extinction curve is too strong in the model S10 without SB3, which suggests that the strength of the 2175 Å bump can depend on whether the SMC experi-

ences SB3 with dust wind. These results thus confirm that the last SB with strong dust wind about 0.2 Gyr ago is a key physical process for the observed characteristic extinction curve of the SMC. The results of the SMC models with different strengths of starbursts are discussed in Appendix B. The metallicity evolution of the SMC (LMC and MW) in the present new models with dust evolution is discussed briefly in Appendix C.

3.2. LMC

Figure 5 presents the time evolution of the extinction curve of the LMC in the model L1 with three SB events. Gas can be more rapidly converted into new stars in this L1 than in the SMC models (owing to the adopted higher SF efficiency) so that chemical abundances can be higher even well before the first SB event ($T = 8.4$ Gyr). As shown in Figure 6, small C- and Si-grains can start to grow earlier in this L1, and their mass fraction can take their peak values before SB1. Consequently, the extinction curve can have a rather conspicuous 2175 Å bump and a very steep FUV rise at $T = 8.4$ and 9.8 Gyr. Since SNe can efficiently destroy dust grains during SB1 owing to high SF rates (i.e. high SN rates), the 2175 Å bump becomes weakened after SB1 ($T = 11.5$ Gyr). However, such destruction of small grains can not severely weaken the 2175 Å bump after SB1 and even after SB2 ($T = 12.5$ Gyr).

The 2175 Å bump of the LMC becomes less conspicuous during SB3 owing to the combination effect of dust destruction and radiation-driven dust wind ($T = 12.9$ Gyr). The shape of the extinction curve of the LMC can not become quite similar to the observed one until the end of SB3 ($T = 13$ Gyr). The rather weak 2175 Å bump at $T = 13$ Gyr in this model is due to the more preferential removal of small C-grains from the LMC through radiation-driven dust wind during the longer starburst (SB3). The major difference in the dust abundances between this LMC model L1 and the SMC model S1 is that the final fractions of small and large C-grains are both slightly larger in L1 than in S1 (See Figures 4 and 6). These differences can cause a difference in the extinction curves between the LMC and the SMC in the present study.

Figure 7 compares between the extinction curve of L1 with dust wind and that of L2 without dust wind. Clearly, L1 with dust wind can better reproduce the observed extinction curve of the LMC, which confirms that the efficient removal of C-grains through radiation driven dust wind is essential for explaining the origin of the extinction curve of the LMC. Previous numerical simulations of the MCs (e.g., Yoshizawa & Noguchi 2003; Bekki & Chiba 2005) suggested that the observed enhanced star formation rates in the MCs (e.g., Harris & Zaritsky 2006, 2009) can be due largely to the LMC-SMC-Galaxy tidal interaction in the past 3 Gyr. Thus the results in Figures 2-7 suggest that the origin of the observed extinction curves of the LMC and the SMC can be closely associated with the past active star formation triggered by tidal interaction among the three galaxies.

3.3. MW

It is instructive for the present study to show whether the new models for dust evolution of galaxies can repro-

duce the observed extinction curve of the MW just by changing the model parameters. Figure 8 describes the time evolution of the MW model M1 without starburst events (thus without dust wind). In the very early chemical evolution history of the model M1 ($T = 1$ Gyr), the extinction curve is rather flat without the clear 2175 Å bump owing to the very small fraction of small C-grains. The extinction curve of the model M1 evolves to have the 2175 Å bump and a steeper rise at $1/\lambda > 6 \mu\text{m}^{-1}$ only 2 Gyr after the commencement of its star formation (i.e., disk formation). The overall feature of the extinction curve becomes quite similar to the observed one for the MW at $T = 5$ Gyr, which implies that MW-like galaxies at higher redshifts might already have extinction curves similar to that of the present MW.

The 2175 Å bump is a bit too conspicuous at $T = 5$ Gyr in comparison with the observed one, and the bump does not evolve significantly with time after $T = 5$ Gyr. This is mainly because the relative mass fractions of small Si-grains and small and large C-grains (with respect to large Si-grains) do not change significantly after $T = 5$ Gyr. The overall shape of the extinction curve at $T = 13$ Gyr becomes closer to that of the observed one. However, the final shape of the 2175 Å bump is still slightly different from the observed one (e.g., more remarkable bump), which implies that the present models do not reproduce the dust abundances of the MW completely well. It is our future study to reproduce better the observed extinction curve of the MW by using a more sophisticated dust evolution model.

These results imply that luminous disk galaxies like the MW are likely to show clear 2175 Å bumps in their extinction curves, because a significant amount of dust is unlikely to be removed from the galaxies owing to their deep gravitational potential. Although a small amount of dust and metals could be removed/ejected from the galaxies through SN and dust wind, such a less significant removal/ejection process can not influence the shapes of the extinction curves to a large extent. The present study therefore predicts that the shapes of extinction curves depend on the masses of galaxies in such a way that more massive galaxies are likely to have the 2175 Å bump. It is an interesting observational question how the strength of the 2175 Å bump in a massive galaxy depends on its physical parameter (e.g., total mass and luminosity). It is worth noting here that Asano et al. (2014) and Nozawa et al. (2015) attempted to reproduce the 2175 Å bump of the MW by freely changing the mass fractions of various ISM phases.

Finally, Figure 9 summarizes the time evolution of mass fractions of the key three dust grains with respect to large Si-grains for the MCs and the MW. The differences in the evolution between the three galaxies can be clearly seen, which reflects on the time evolution of the extinction curves of the three. Star formation histories with or without starbursts and capabilities to retain dust within galaxies are key determinant for the time evolution of the extinction curves of galaxies. Since the present study has investigated only three different types of galaxies (i.e., SMC, LMC, and MW), we will need to investigate models with different star formation and dust evolution histories to understand fully the origin of various extinction curves ob-

served in galaxies with different masses and Hubble types.

4. DISCUSSION

4.1. The origin of the 2175 Å bump

We have, for the first time, demonstrated that the observed extinction curve without the 2175 Å bump in the SMC can be reproduced, if the small C-grains can be more preferentially lost through radiation-driven wind during the last starburst around 0.2 Gyr ago. In this “lost small C-grain” scenario, the LMC can have a weak 2175 Å bump in its dust extinction curve, because it can retain a larger amount of small C-grains owing to its deeper gravitational potential in comparison with the SMC. This “lost small C-grain” scenario predicts that more massive galaxies (like the MW) are likely to show more distinctive 2175 Å bumps in their dust extinction curves. It should be stressed, however, that the present low-mass galaxies can show such 2175 Å bumps if they have not experienced recent strong starbursts and the resultant loss of small C-grains.

The key physical process required for the lack of the 2175 Å bump in a galaxy is the more efficient removal of C-grains than Si-grains from the galaxy. The removal (or stripping) process of dust grains in galaxies should be rather complicated, because gravitational dynamics, gas-dust drag, and radiation pressure of stars can be all involved in the removal process. Therefore, it would be a formidable task to estimate accurately the dust removal efficiency in a galaxy for the physical parameters of the galaxy. Thus we investigate whether and in what physical conditions the above two requirements can be met in a galaxy by using a simplified yet reasonable model.

The first question is whether these C-grains can be more efficiently removed from a galaxy through radiation-driven wind than Si-grains. The key parameter for this removal process in a galaxy is the frequency-averaged radiation pressure coefficient (Q_{pr}^*), as demonstrated in previous theoretical models and recent numerical simulations of dust wind in galaxies (e.g., Ferrara et al. 1991; Bianchi & Ferrara 2005; Bekki 2015). We have therefore investigated Q_{pr}^* for C and Si grains by using the publicly available data for optical properties of dust (Draine and Lee 1984; Laor & Draine 1993) and the stellar population synthesis code (“MILES”) developed by Vazdekis et al. (2010). The radiation pressure coefficient (Q_{pr}) for a grain with a radius is given as follows:

$$Q_{\text{pr}} = Q_{\text{abs}} + (1 - g(\theta))Q_{\text{sca}}, \quad (30)$$

where Q_{abs} and Q_{sca} are the absorption and scattering coefficient, respectively, and $g(\theta)$ is the scattering asymmetry parameter.

Using Q_{pr} and the flux of a SED ($f(\lambda)$), we can estimate Q_{pr}^* as follows:

$$Q_{\text{pr}}^* = \int_{\lambda_{\text{min}}}^{\lambda_{\text{max}}} Q_{\text{pr}} f(\lambda) d\lambda, \quad (31)$$

where λ_{min} and λ_{max} are set to be 3340.5 Å and 7409.6 Å, respectively, in MILES. The above wavelength range is publicly available one in MILES and $f(\lambda)$ is the normalized flux (i.e., $\int_{\lambda_{\text{min}}}^{\lambda_{\text{max}}} f(\lambda) d\lambda = 1$). Figure 10 shows the wavelength-dependence of radiation pressure coefficient (Q_{pr}) for silicate and graphite with the radii of 0.01

μm and $0.1\mu\text{m}$ and the SED of a galaxy for a metallicity ($[Z/H]$) of -0.7 dex and an age of 63 Myr (which is the youngest stellar population that can be adopted in MILES). We use this SED for a single stellar population (SSP) to mimic the SMC with young starburst components. We discuss just this model with two representative dust radii as an example, though, ideally speaking, we should show the results for all dust radii.

Clearly, Q_{pr}^* is higher in graphite than in silicate for the adopted SED and dust radii ($0.01\mu\text{m}$ and $0.1\mu\text{m}$), which means that graphite is more likely to be influenced by radiation pressure of stars and thus removed from a galaxy if the gravitational potential is sufficiently shallow. Furthermore, the difference in Q_{pr}^* is significantly larger in the small grains ($a = 0.01\mu\text{m}$) than in the large ones ($a = 0.1\mu\text{m}$), which implies that small C-grains can be much more efficiently removed than small Si-grains. Although the real SED of a SMC-type galaxy might be different from the adopted SED in this investigation, it is unlikely that this result changes qualitatively if a more realistic SED is adopted, given Q_{pr} of graphite always higher than those of silicate for the relevant wavelength range. These results thus suggest that graphite is more likely to be lost from a SMC-type galaxy than silicate, though a full investigation on this dust removal process for different dust grains and more realistic galaxy spectra needs to be done in our future studies.

If a rather small mass fraction of small C-grains is responsible for the observed lack of the 2175 \AA bump in the SMC, then is there any observational evidence for that? Using ISOPHOTO and HiRes IRAS data for dust emission and ATCA data for HI column gas density, Bot et al. (2004) investigated the gas-to-dust-ratios of polycyclic aromatic hydrocarbon (PAH) molecules or small grains (VSGs) for different regions of the SMC. They found that the derived difference in the gas-to-dust-ratio of PAHs and very small grains between the Galaxy and the SMC is three times larger than the metallicity difference between the two galaxies. This observational result implies that the dust depletion levels for VSG and PAHs are low in the SMC for some physical reasons (e.g., destruction by SNe; Bot et al. 2004). Since this observational study can not distinguish small C-grains from small Si-grains, it is not clear whether the observed low depletion level of VSGs implies that the mass fraction of small C-grains is significantly low owing to efficient removal or destruction of such grains. It appears to be difficult for photometric study of the SMC alone to estimate the contributions of small C- and Si-grains to the observed dusty SED separately.

The present study predicts that the star-forming regions of the SMC for which there is no 2175 \AA bump can be dominated by Si-grains (i.e., small fractions of C-grains). However, Welty et al. (2001) found that the Si appears to be *undepleted* in a local region of the SMC toward the SMC star Sk 155, which means that the local region should contain little Si dust. If this is not just for the Sk 155 region but for other star-forming regions generally in the SMC, then the present scenario and other dust models for the SMC like Pei (1992) appears to be ruled out. Thus it would be observationally important to make a robust estimation of the dust depletion level of Si in many star-forming regions with and without the 2175 \AA bump for

the SMC.

4.2. Alternative scenarios

A number of possible carriers of the 2175 \AA bump have been extensively discussed by many authors so far (e.g., Whittet 2003). Mishra & Li (2015) have recently found a strong correlation between the strength of the 2175 \AA bump and the carbon depletion level ($[C/H]_{\text{dust}}$) in the MW and thus suggested that the carrier of the observed 2175 \AA bump is graphite or PAH molecules. Their results are consistent with the present “lost small C-grains” scenario, though they did not discuss small and large C-grains separately in the context of the origin of the 2175 \AA bump. The results imply that the time evolution of C-grains in a galaxy can be reflected on the strength of the 2175 \AA bump in the extinction curve of the galaxy.

The severely deficient small C-grain of the SMC ISM discussed in the present study would be just one of the promising ways that explain the observed lack of the 2175 \AA bump in the SMC. Nozawa et al. (2015) have recently reproduced the observed dust extinction curve without the 2175 \AA bump in SDSS J1048+4637 by adopting the optical constant of amorphous carbon for carbonaceous grains (See Figure 4 in their paper). Although their dust extinction curve (Nozawa et al. 2015) is quite different from that of the SMC, it would be possible that amorphous carbon dust might be responsible for the lack of the 2175 \AA bump in the SMC extinction curve. Recent observational study of dust in the LMC by Herschel (Meixner et al. 2010) has shown that their dust model with amorphous carbon can better explain their observations for a more reasonable dust-to-gas-ratio. It appears to be currently difficult to model the evolution of amorphous carbon by considering the possible physical effects (e.g., radiation fields and gaseous shock) related to the transformation of carbon grain properties.

As demonstrated in the present study, a way to reproduce the observed lack of the 2175 \AA bump in the SMC extinction curve is to reduce the relative contribution of small C-grains. Therefore, it does not make much difference whether small C-grains can be lost either through energetic dust wind or through some destruction process of dust grains. If small C-grains can be more preferentially destroyed or transformed by SNe or gaseous shock or strong radiation field in the ISM of the SMC, the 2175 \AA bump might not be observed in the SMC. It would be possible that the last strong LMC-SMC collision/interaction about 0.2 Gyr ago (e.g., Diaz & Bekki for the latest model), which can strongly compress the ISM of the SMC (e.g., Bekki & Chiba 2007), could preferentially destroy the small C-grains. It is our future study to investigate whether small C-grains can be more preferentially destroyed by these physical processes in the ISM by using pc-scale numerical simulations of the ISM.

4.3. Incorporation of four-component grain models into numerical simulations of galaxy formation and evolution

Interstellar dust can have significant influences on the physical processes of galaxy formation and evolution, such as the formation of molecular hydrogen in the ISM of galaxies (e.g., Gould & Salpeter 1963) and photo-

electric heating of the ISM (e.g., Watson 1972). Although these influences have been recently included in Nbody+hydrodynamical simulations of galaxy formation and evolution in a self-consistent manner (Bekki 2013, 2014, and 2015), the evolution of dust sizes, which can control dust-related physical processes of ISM (e.g., Yamasawa et al. 2011), has not been incorporated properly into numerical simulations of galaxy formation and evolution. The present study has demonstrated that the evolution of dust sizes and compositions is a key factor for the evolution of extinction curves in galaxies. We thus suggest that if future numerical simulations of galaxy formation and evolution can include the time evolution of dust sizes and compositions, such numerical studies can have the following improvements in their predictive power.

First, such simulations with the evolution of dust sizes and compositions can predict the SEDs of galaxies in a more consistent manner. The SEDs of dusty galaxies are strongly influenced by the adopted extinction curves, and the shapes of the extinction curves of galaxies depend on their star formation histories that control their dust evolution histories. Therefore, previous SED models of galaxies with a fixed extinction curve (e.g., an adoption of the MW dust extinction curve) might be much less self-consistent and realistic. Construction of SEDs from age and metallicity distributions of stars and spatial distributions of stars in numerical simulations has been done by many authors (e.g., Bekki et al. 1999; Bekki Shioya 2001; Johnson 2006; Yajima et al. 2014), though they had to assume a constant dust-to-metal-ratio and a fixed dust extinction curve. It is doubtlessly worthwhile for these simulations to include the evolution of dust sizes and compositions for a more consistent prediction of galactic SEDs.

Second, future simulations with dust size evolution can provide more accurate predictions of molecular hydrogen abundances in the ISM of galaxies. As shown in sophisticated one-zone models of galaxy formation with dust size evolution by Yamasawa et al. (2012), the formation efficiency of molecular hydrogen on dust grains in a forming galaxy depends on the evolution of the dust size distribution of the galaxy: since the molecular hydrogen formation rate on the surface of a dust grain depends on the surface area, the net formation rate of molecular hydrogen on dust grains in a galaxy relates to the dust extinction curve. In order for numerical simulations to predict the dust size distribution of a galaxy, they need to follow the time evolution of dust grains with different sizes for each gas particle. This is a very formidable task, because such dust grain evolution is computationally heavy even in one-zone chemical evolution models (e.g., Asano et al. 2014). A wise way to implement the dust size evolution in numerical simulations of galaxy formation would be to adopt a two-size approximation as done in this study.

Third, the effects of photo-electric heating of dust on the thermal evolution of ISM in galaxies can be more self-consistently investigated in numerical simulations with dust size evolution. The photo-electric heating rate depends on the dust size distribution (not just dust abundances), and the photo-electric heating has been demonstrated to influence galaxy-wide star formation through its influences on thermal history of galactic ISM (e.g., Bekki 2015). Therefore photo-electric heating would be one of

the key ingredients that future numerical simulations, in particular, those for the evolution of galaxy-wide star formation, should include. Thus, we suggest that incorporation of dust size evolution into numerical simulations of galaxy formation and evolution is essential for understanding various aspects of galaxy formation and evolution.

5. CONCLUSIONS

We have constructed a new dust evolution model for the MCs by incorporating the two-size (i.e., small and large) approximation model for dust size distributions (H15) into one-zone chemical evolution models with dust winds. The time evolution of small and large dust grains has been self-consistently investigated for each element (e.g., C, O, and Si) by considering shattering and coagulation of these grains. The extinction curve of a galaxy at each time step in a one-zone chemical evolution model has been derived from the relative abundances of small and large carbonaceous grains ('C-grains') and small and large silicate grains ('Si-grains') by using the optical constants for these grains: the galaxy has four-component dust in the ISM. We have searched for the model parameters with which the observed extinction curves of the MCs can be successfully reproduced. However, we mainly showed the results of the models with different wind parameters to demonstrate more clearly the key roles of dust wind in the evolution of dust extinction curves. The main results are as follows.

(1) The SMC extinction curve with almost no 2175 Å bump and a rather steep FUV rise can be reproduced well by the present models with SFHs consistent with the observed ones ('SMC model'), if the small C-grains can be more efficiently ejected from the SMC through radiation-driven dust wind during the latest starburst about 0.2 Gyr ago. Without this selective loss of small C-grains, the models show conspicuous 2175 Å feature regardless of model parameters for SFHs and dust physics. These results suggest that the significantly enhanced star formation possibly triggered by the last LMC-SMC tidal interaction can be responsible for the origin of the 2175 Å bump in the SMC.

(2) The LMC extinction curve with weak 2175 Å bump and a steeper FUV rise can be also reproduced by the present LMC models, if the small C-grains can be ejected from the LMC more efficiently than other dust components. The dust removal efficiency of small C-grains required to explain the LMC extinction curve should be by a factor of ~ 3 smaller than that required to explain the SMC extinction curve. Such a less efficient ejection of small C-grains is possible for the LMC owing to the deeper gravitational potential well.

(3) The present model can reproduce the extinction curve of the MW with the 2175 Å bump if there is no recent starburst event (as observed) that can trigger strong dust wind in the model. This is simply because small C-grains can not be preferentially lost in the MW model with the quiescent star formation history. We have suggested (i) that dust grains are less likely to be ejected from the MW owing to its deep gravitational potential well (in comparison with the MCs) and (ii) that this more efficient trapping of dust grains in the MW can be responsible for the evolution of the extinction curve.

(4) The selective loss of small C-grains from the ISM of

the MCs is demonstrated to be physically reasonable and realistic, because the frequency-averaged radiation pressure efficiency (Q_{pr}^*) is significantly larger in small C-grains than in small Si-grains for reasonable spectral energy distributions of the MCs. Since there are other alternative mechanisms for the origin of the extinction curves of the MCs with no/little 2175 Å bump (e.g., selective destruction of small C-grains and amorphous carbon grains in the MCs), these alternative scenarios will need to be investigated in our future papers.

(5) The present study suggests that the dust extinction curves could be different between galaxies with different masses (i.e., difference in the depth of gravitational potential) and different star formation histories (e.g., with or without starbursts), because the evolution of dust composition and size distributions can be influenced by these physical properties of galaxies. We will need a full numerical simulation including most of the dust-related physical processes in order to understand the dependences of the

dust extinction curves on the physical properties of galaxies.

The strength of the 2175 Å bump, their correlations with galaxy properties, and the influence of the bump on galactic SEDs have been investigated for galaxies with different masses and types at low and high redshifts (e.g., Calzetti et al. 1994; Noll et al. 2009; Inoue et al. 2006; Conroy 2009; Buat et al. 2011; Wild et al. 2011; Kriek & Conroy 2013; Mao et al. 2014; Scoville et al. 2015). Although the present study did not discuss these observations, the new results based on the present dust wind model can provide some clues to the origin of these observed properties. We will discuss these issues in our forthcoming papers.

We are grateful to the anonymous referee for constructive and useful comments. HH thanks the support from the Ministry of Science and Technology (MoST) grant 102-2119-M-001-006-MY3.

REFERENCES

- Asano, R. S., Takeuchi, T. T., Hirashita, H., & Nozawa, T. 2013, *MNRAS*, 432, 637
- Asano, R. S., Takeuchi, T. T., Hirashita, H., & Nozawa, T. 2014, *MNRAS*, 440, 134
- Bekki, K. 2013, *MNRAS*, 432, 2298
- Bekki, K. 2014, *MNRAS*, 444, 1615
- Bekki, K. 2015, *MNRAS*, 449, 1625
- Bekki, K., Shioya, Y., & Tanaka, I. 1999, *ApJ*, 520, L99
- Bekki, K., & Shioya, Y. 2001, *ApJS*, 134, 241
- Bekki, K., & Chiba, M. 2005, *MNRAS*, 356, 680
- Bekki, K., & Chiba, M. 2007, *PASA*, 24, 21
- Bekki, K., & Tsujimoto, T. 2010, *ApJ*, 721, 1515
- Bekki, K., & Tsujimoto, T. 2012, *ApJ*, 761, 180 (BT12)
- Bekki, K., & Tsujimoto, T. 2014, *MNRAS*, 444, 3879 (BT14)
- Bianchi, S., & Ferrara, A. 2005, *MNRAS*, 358, 379
- Bohren, C. F., & Huffman, D. R. 1983, *Absorption and scattering of light by small particles*, New York Wiley
- Bot, C., Boulanger, F., Lagache, G., Cambresy, L., & Egret, D. 2004, *A&A*, 423, 567
- Bromage, G. E., & Nandy, K. 1983, 204, 29
- Buat, V., et al. 2011, *A&A*, 533, 93
- Calzetti, D., Kinney, A. L., & Storchi-Bergmann, T. 1994, *ApJ*, 429, 582
- Carrera, R., Gallart, C., Aparicio, A., Costa, E., Mendez, R. A., & Noel, N. E. D. 2008, *AJ*, 136, 1039
- Cioni, M., et al. 2014, *A&A*, 562, 32
- Clayton, G. C., & Martin, P. G. 1985, *AJ*, 288, 558
- Cole, A. A., Tolstoy, E., Gallagher, J. S. III., & Smecker-Hane, T. A. 2005, *AJ*, 129, 1465
- Conroy, C. 2010, *MNRAS*, 404, 247
- Corbelli, E., 2012, *A&A*, 542, 32
- Da Costa, G. S., & Hatzidimitriou, D. 1998, *AJ*, 115, 1934
- Diaz, J., & Bekki, K. 2011, *MNRAS*, 413, 2015
- Diaz, J., & Bekki, K. 2012, *ApJ*, 750, 36
- Dobbie, P. D., Cole, A. A., & Subramaniam, A., & Keller, S. 2014, *MNRAS*, 442, 1663
- Draine, B. T., & Lee, H. M. 1984, *ApJ*, 285, 89
- Dwek, E., 1998, *ApJ*, 501, 643
- Ferrara, A., Ferrini, F., Barsella, B., Franco, J., 1991, *ApJ*, 381, 137
- Fitzpatrick, E. 1985, *ApJ*, 299, 219
- Fitzpatrick, E. 1989, *Interstellar Dust* Edited by Louis J. Allamandola and A. G. G. M. Tielens. International Astronomical Union. Symposium no. 135, Kluwer Academic Publishers, Dordrecht, p.37
- Galliano, F., et al. 2011, *A&A*, 536, 88
- Gardiner, L. T. & Noguchi, M. 1996, *MNRAS*, 278, 191
- Gordon, K. D., & Clayton, G. C. 1998, *ApJ*, 500, 816
- Gordon, K. D., Clayton, G. C., Misselt, K. A., Landolt, A. U., Wolff, M. J. 2003, *ApJ*, 594, 279
- Gould, R. J., Salpeter, E. E., 1963, *ApJ*, 138, 393
- Harris J., & Zaritsky D. 2006, *AJ*, 131, 2514
- Harris J., & Zaritsky D. 2009, *AJ*, 138, 1243
- Hirashita, H. 2015, *MNRAS*, 447, 2937 (H15)
- Hou, K. C., & Hirashita, H. 2015, in preparation
- Hutchings, J. B. 1982, *ApJ*, 255, 70
- Inoue, A. K., Buat, V., Burgarella, D., Panuzzo, P., Takeuchi, T. T., & Iglesias-Paramo, J. 2006, *MNRAS*, 370, 380
- Jonsson, P., 2006, *MNRAS*, 372, 2
- Kallivayalil, N., van der Marel, R. P., Alcock, C., Axelrod, T., Cook, K. H., Drake, A. J., Geha, M., 2006, *ApJ*, 638, 772
- Kaneda, H., Ishihara, D., Suzuki, T., Ikeda, N., Onaka, T., Yamagishi, M., Ohyama, Y., Wada, T., & Yasuda, A. 2010, *A&A*, 514, 14
- Kennicutt, R. C., Jr., Bresolin, F., Bomans, D. J., Bothun, G. D., & Thompson, I. B. 1995, *AJ*, 109, 594
- Kim, S., Dopita, M. A., Staveley-Smith, L., & Bessel, M. 1999, *AJ*, 118, 2823
- Kriek, M., & Conroy, C. 2013, *ApJ*, 775, L16
- Laor, A., & Draine, B. T. 1993, *ApJ*, 402, 441
- Mishra, A., & Li, A., 2015 (preprint)
- Mao, Y.-W., Kong, X., & Lin, L. 2014, *ApJ*, 789, 76
- Mao, D., Sharon, K., Gal-Yam, A., 2010, *ApJ*, 722, 1879
- Matsuura, M., et al. 2011, *Sci*, 333, 1258
- Meixner, M., et al. 2010, *A&A*, 518, L71
- Nandy, K., McLachlan, A., Thompson, G. I., Morgan, D. H., Willis, A. J., Wilson, R., Gondhalekar, P. M., & Houziaux, L. 1982, *MNRAS*, 201, 1
- Nidever, D. L., Majewski, S. R., Munoz, R. R., Beaton, R. L., Patterson, R. J., Kunkel, W. E. 2011, *ApJ*, 733, L10
- Noll, S., et al. 2009, *A&A*, 499, 69
- Nozawa, T., Asano, R. S., Hirashita, H., & Takeuchi, T. T. 2015, *MNRAS*, 447, L16
- Pei, Y. C. 1992, *ApJ*, 395, 130
- Piatti, A. E., Santos, J. F. C., Claria, J. J., Bica, E., Sarajedini, A., & Geisler, D. 2001, *MNRAS*, 325, 792
- Prevot, M. L., Lequeux, J., Prevot, L., Maurice, E., & Rocca-Volmerange, B. 1984, *A&A*, 132, 389
- Rocca-Volmerange, B., Prevot, L., Prevot-Burnichon, M. L., Ferlet, R., & Lequeux, J. 1981, *A&A*, 99, L5
- Rubele, S., et al. 2012, *A&A*, 537, 106
- Rubele, S., et al. 2015, *MNRAS*, 449, 639
- Salpeter, E. E. 1955, *ApJ*, 121, 161
- Savage, B. D., & Mathis, J. S. 1979, *ARA&A*, 17, 73
- Scoville, N., Faisst, A., Capak, P., Kakazu, Y., Li, G., & Steinhardt, C. 2015, *ApJ*, 800, 108
- Schneider, R., Valiante, R., Ventura, P., dell'Agli, F., Di Criscienzo, M., Hirashita, H., & Kemper, F. 2014, *MNRAS*, 442, 1440
- Stanimirovic, S., Staveley-Smith, L., Dickey, J. M., Sault, R. J., & Snowden, S. L. 1999, *MNRAS*, 302, 417
- Stanimirovic, S., Staveley-Smith, L., Jones, P. A. 2004, *ApJ*, 604, 176
- Tsujimoto, T., Nomoto, K., Yoshii, Y., Hashimoto, M., Yanagida, S., & Thielemann, F.-K. 1995, *MNRAS*, 277, 945 (T95)
- Tsujimoto, T., & Bekki, K. 2009, *ApJ*, 700, L69
- Tsujimoto, T., Bland-Hawthorn, J., & Freeman, K. C. 2010, *PASJ*, 62, 447
- van den Bergh, S. *The Galaxies of the Local Group*.
- van den Hoek, L. B., & Groenewegen, M. A. T. 1997, *A&AS*, 123, 305 (VG97)
- Vazdekis, A., et al. 2010, *MNRAS*, 404, 1639

- Watson, W. D., 1972, *ApJ*, 176, 103
Weidemann, V. 2000, *A&A*, 363, 647
Weingartner, J. C., & Draine, B. T. 2001, *ApJ*, 553, 581
Welty, D. E., Lauroesch, J. T., Blades, J. C., Hobbs, L. M., & York, D. G. 2001, *ApJ*, 554, L75
Westerland, B. E. 1997, *The Magellanic Clouds*, Cambridge University press
Wild, V., Charlot, S., Brinchmann, J., Heckman, T., Vince, O., Pacifici, C., & Chevallard, J. 2011, *MNRAS*, 417, 1760
Whittet, D. C. B. 2003, *Dust in the Galactic Environment* (2nd edn.)
Yajima, H., Nagamine, K., Thompson, R., & Choi, J.H. 2014, *MNRAS*, 439, 3073
Yamasawa, D., Habe, A., Kozasa, T., Nozawa, T., Hirashita, H., Umeda, H., & Nomoto, K. 2011, *ApJ*, 735, 44
Yoshizawa, A. M., & Noguchi, M. 2003, *MNRAS*, 339, 1135
Yozin, C., & Bekki, K. 2014, *MNRAS*, 443, 522
Zhukovska, S., & Henning, T. 2013, *A&A*, 555, 99

TABLE 1
THE MODEL PARAMETERS FOR SF HISTORIES OF THE THREE GALAXIES.

Galaxy name	C_q ^a	C_{sb1} ^b	C_{sb2} ^c	C_{sb3} ^d	$t_{sb1,s}$ ^e	$t_{sb1,e}$ ^f	$t_{sb2,s}$ ^g	$t_{sb3,e}$ ^h	$t_{sb3,s}$ ⁱ	$t_{sb3,e}$ ^j
SMC	0.005	0.05	0.05	0.1	8.5	8.6	11.5	11.6	12.85	12.99
LMC	0.01	0.05	0.05	0.1	10.0	10.1	11.5	11.6	12.85	12.99
MW	0.06	-	-	-	-	-	-	-	-	-

^aThe star formation coefficient (C_{sf}) during the quiescent phase (i.e., without starburst).

^b C_{sf} during the first starburst phase (SB1). The mark “-” in the MW model means C_{sf} is always C_q owing to no starburst events.

^c C_{sf} during the second SB phase (SB2).

^d C_{sf} during the third starburst phase (SB3).

^eThe time (Gyr) when the first SB starts. The mark “-” in the MW model means no SB events in its star formation history.

^fThe time (Gyr) when the first SB ends.

^gThe time (Gyr) when the second SB starts.

^hThe time (Gyr) when the second SB ends.

ⁱThe time (Gyr) when the third SB starts.

^jThe time (Gyr) when the third SB ends.

TABLE 2
 THE MODEL PARAMETERS FOR THE TIMESCALES FOR THE INVESTIGATED PHYSICAL PROCESSES OF DUST.

Physical process	Parameter ^a	small Si ^b	large Si	small C	large C
Accretion	$\tau_{\text{acc},\odot}$	0.02	0.2	0.02	0.2
Destruction	$\tau_{\text{SN},\odot}$	0.2	0.2	0.2	0.2
Shattering	$\tau_{\text{sh},\odot}$	-	0.1	-	0.1
Coagulation	$\tau_{\text{co},\odot}$	0.2	-	0.2	-

^aA simple version of the parameter description is given (e.g., τ_{acc} instead of $\tau_{\text{acc},i,j}$). The value for each parameter (e.g., $\tau_{\text{acc},\odot}$) is for the metal and dust abundances of the solar neighborhood (in the present Galaxy).

^bDust is assumed to consist of four different types of grains: small and large Si-grains and small and large C-grains. The small Si-grain is simply referred to as small Si in this column. Each timescale is given in units of Gyr. The mark “-” means that the listed physical process is not applicable.

TABLE 3
THE MODEL PARAMETERS FOR RADIATION-DRIVEN DUST WIND IN EACH MODEL.

Model name ^a	$C_{w,s,Si}$ ^b	$C_{w,l,Si}$	$C_{w,s,C}$	$C_{w,l,C}$	comments
S1	0.01	0.002	0.05	0.01	fiducial SMC
S2	0.0	0.0	0.0	0.0	no dust wind
S3	0.01	0.002	0.01	0.01	
S4	0.01	0.002	0.03	0.01	
S5	0.01	0.002	0.1	0.01	
S6	-	-	-	-	no SB
S7	0.01	0.002	0.05	0.01	no SB1
S8	0.01	0.002	0.05	0.01	no SB2
S9	0.01	0.002	0.05	0.01	no SB3
L1	0.01	0.002	0.03	0.01	fiducial LMC
L2	0.0	0.0	0.0	0.0	no dust wind
M1	-	-	-	-	fiducial MW

^aThe first capital alphabets “S”, “L”, “M” indicate SMC, LMC, and MW models, respectively. The mark “-” means no dust wind owing to no starburst events whereas the zero value (0.0) means no dust wind in spite of starburst.

^bThe dust removal coefficient for small and large Si-grains and small and large C-grains is represented by $C_{w,s,Si}$, $C_{w,l,Si}$, $C_{w,s,C}$, and $C_{w,l,C}$, respectively.

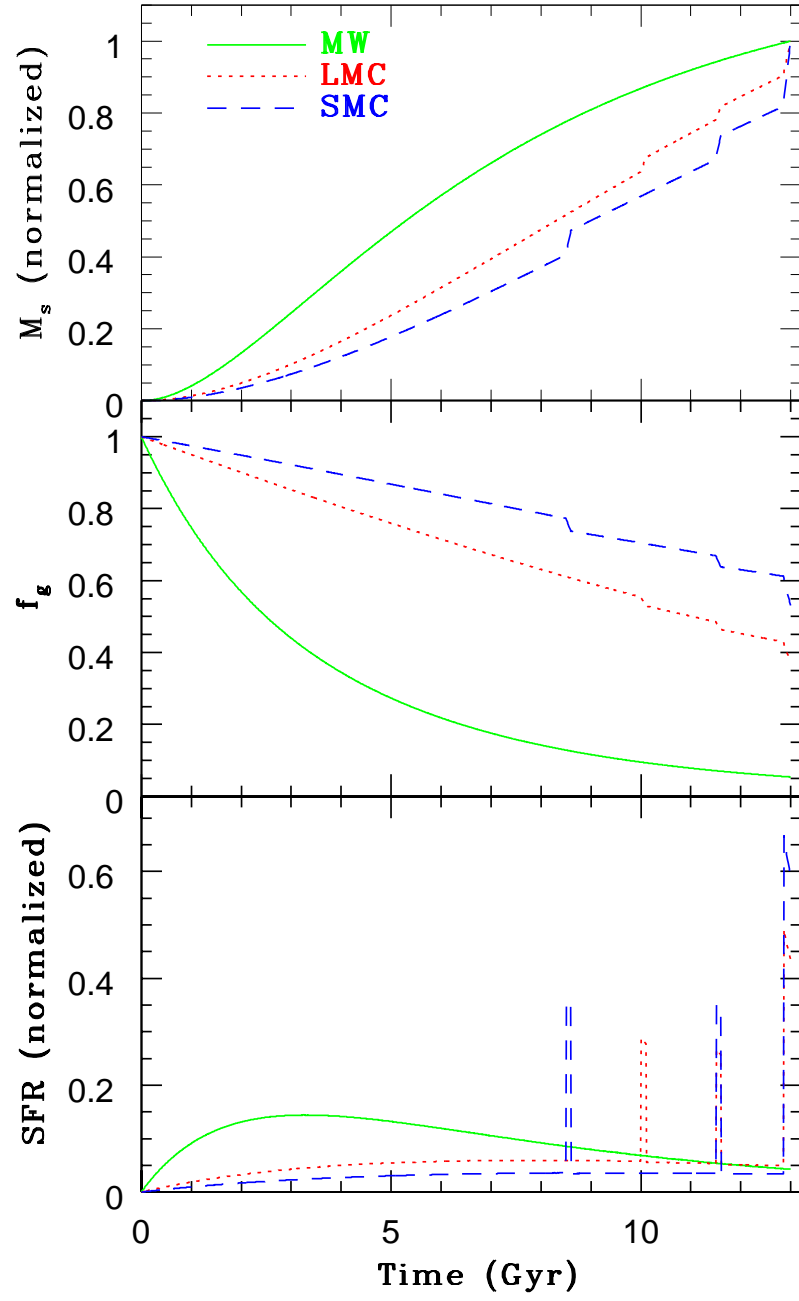


FIG. 1.— Time evolution of the total stellar mass (M_s), gas mass fraction (f_g), and SFR for the MW (green solid), the LMC (red dotted), and the SMC (blue dashed). The SFR at each time step is the “normalized” one so that we can compare the time evolution of SFRs between the three galaxies more clearly. The normalized SFR is given in units of $0.1M_{\text{unit}}/t_{\text{unit}}$ just for convenience, where M_{unit} and t_{unit} are mass and time units for a model, respectively, and they are initial gas mass (M_g) and 10^8 yr, respectively.

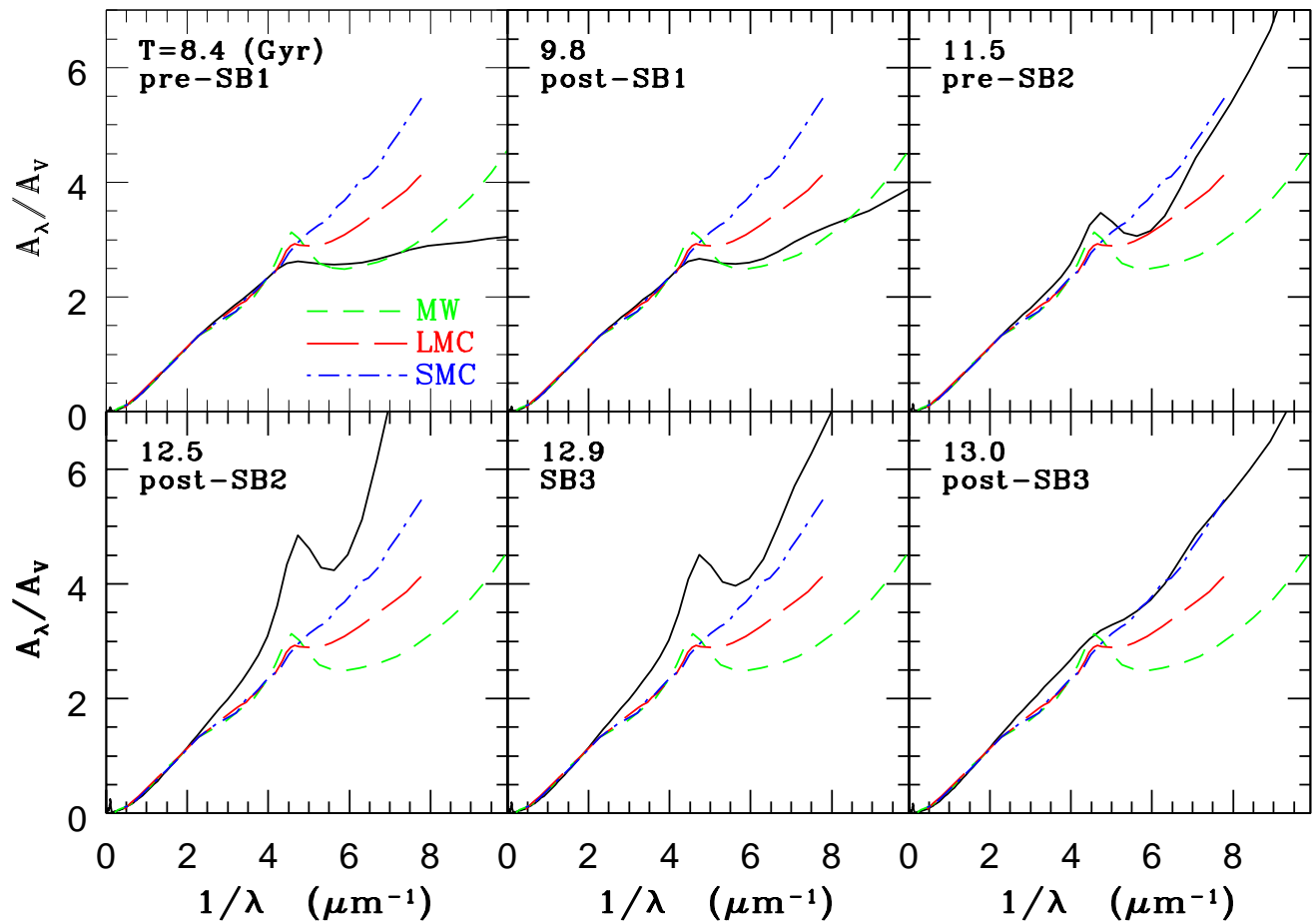


FIG. 2.— Extinction curves of the modeled SMC (black solid) at the selected 6 time steps, $T = 8.4$ Gyr (before the first starburst, “pre-SB1”), $T = 9.8$ Gyr (after the first starburst “post-SB1”), $T = 11.5$ Gyr (“post-SB2”), $T = 12.5$ Gyr (“post-SB2”), $T = 12.9$ Gyr (during the third SB “SB3”), and $T = 13.0$ Gyr (“post-SB3”). For comparison, the observed extinction curves of the MW (green short-dashed), the LMC (red long-dashed), and the SMC (blue dot-dashed) are shown in each frame.

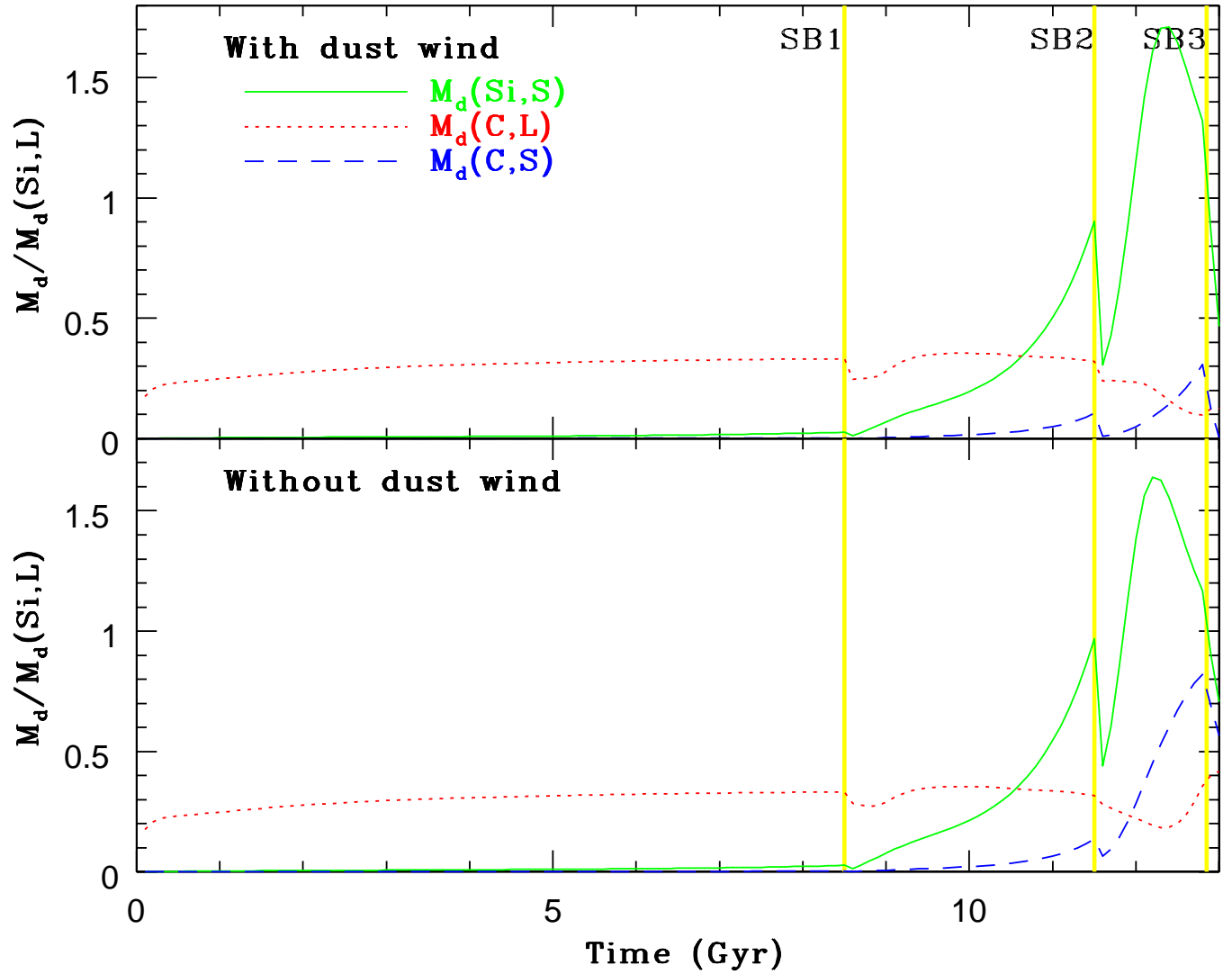


FIG. 3.— Time evolution of the total grain masses (normalized to the total mass of large Si grains at each time step for convenience) for small Si-grains ($M_d(\text{Si},\text{S})$; green solid), large C-grains ($M_d(\text{C},\text{L})$; red dotted), and small C-grains ($M_d(\text{C},\text{S})$; blue dashed) for the SMC model S1 with dust wind (upper) and S2 without dust wind (lower). Three thick yellow lines indicate the epochs of starbursts (SB1, SB2, and SB3).

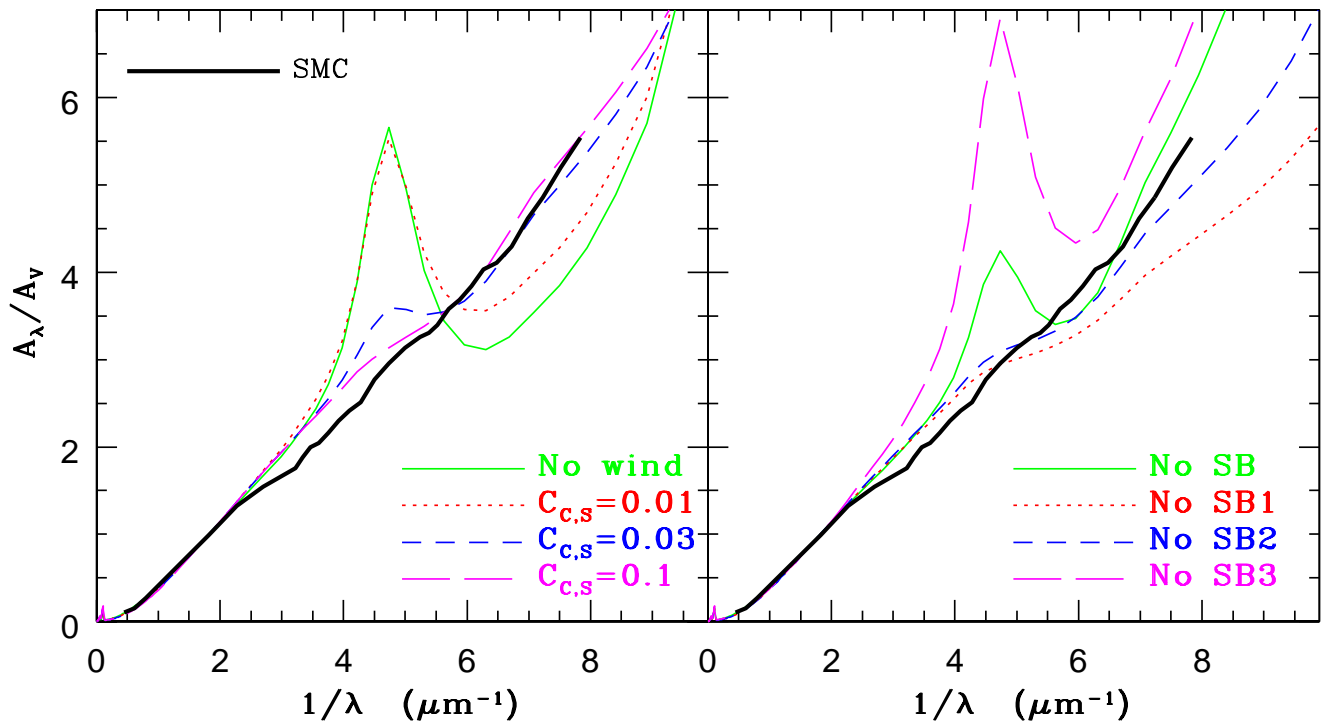


FIG. 4.— Extinction curves for the eight SMC models. The left panel shows S2 with starburst (SB) yet no wind (green solid), S3 with the dust removal efficiency for small C-grains ($C_{w,s,C}$) being 0.01 (red dotted), S4 with $C_{w,s,C} = 0.03$ (blue short-dashed), S5 with $C_{w,s,C} = 0.1$ (magenta long-dashed). The right panel shows S6 with no SB thus no wind (green solid), S7 with no SB1 (yet with SB2 and SB3; red dotted), S8 with no SB2 (blue short-dashed), S9 with no SB3 (magenta long-dashed). The thick black solid line indicates the observed extinction curve of the SMC.

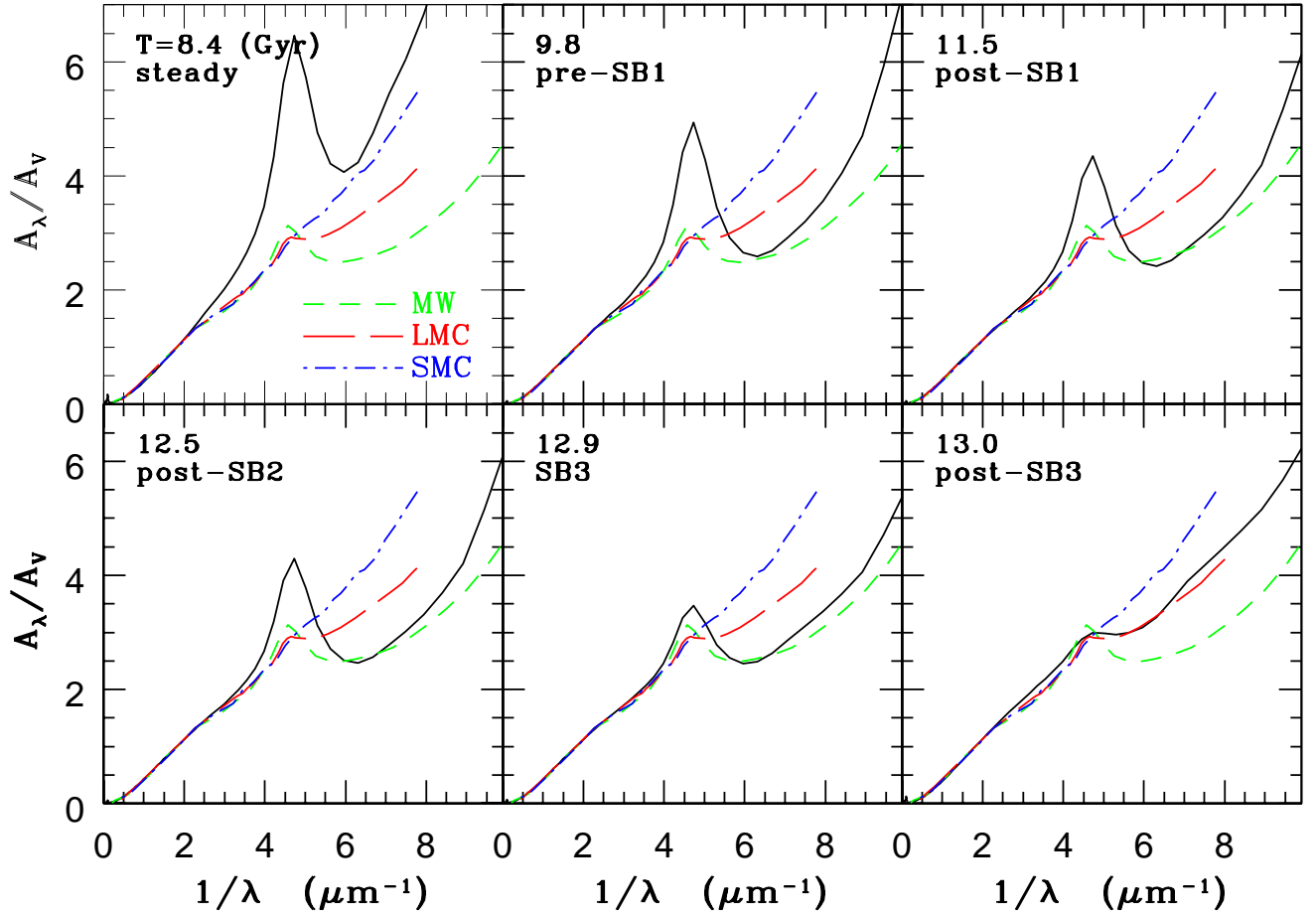


FIG. 5.— Same as Figure 2 but for the LMC model L1. The first starburst epoch (SB1) is different between this model L1 and S1.

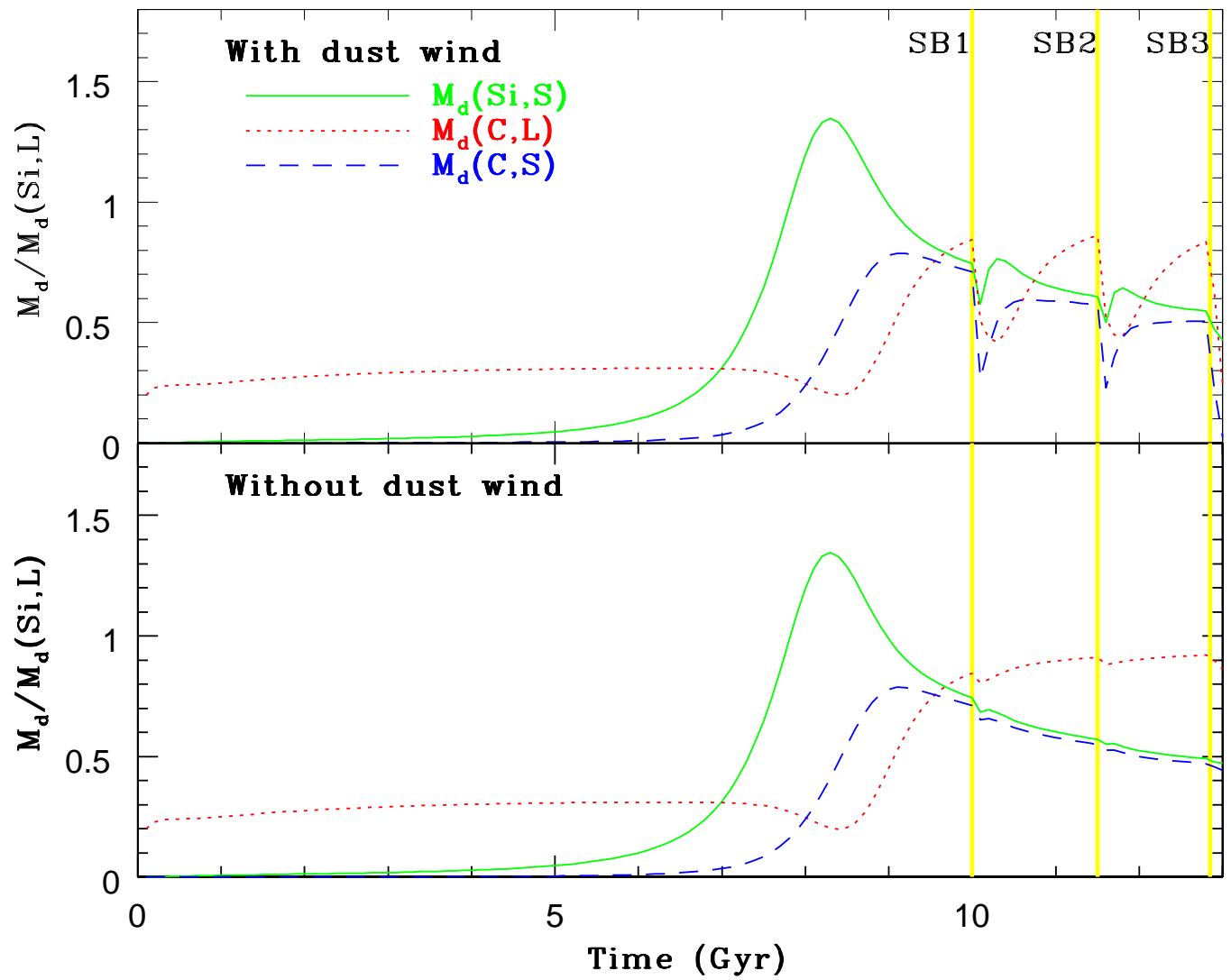


FIG. 6.— Same as Figure 3 but for the LMC models with (L1) and without (L2) dust wind.

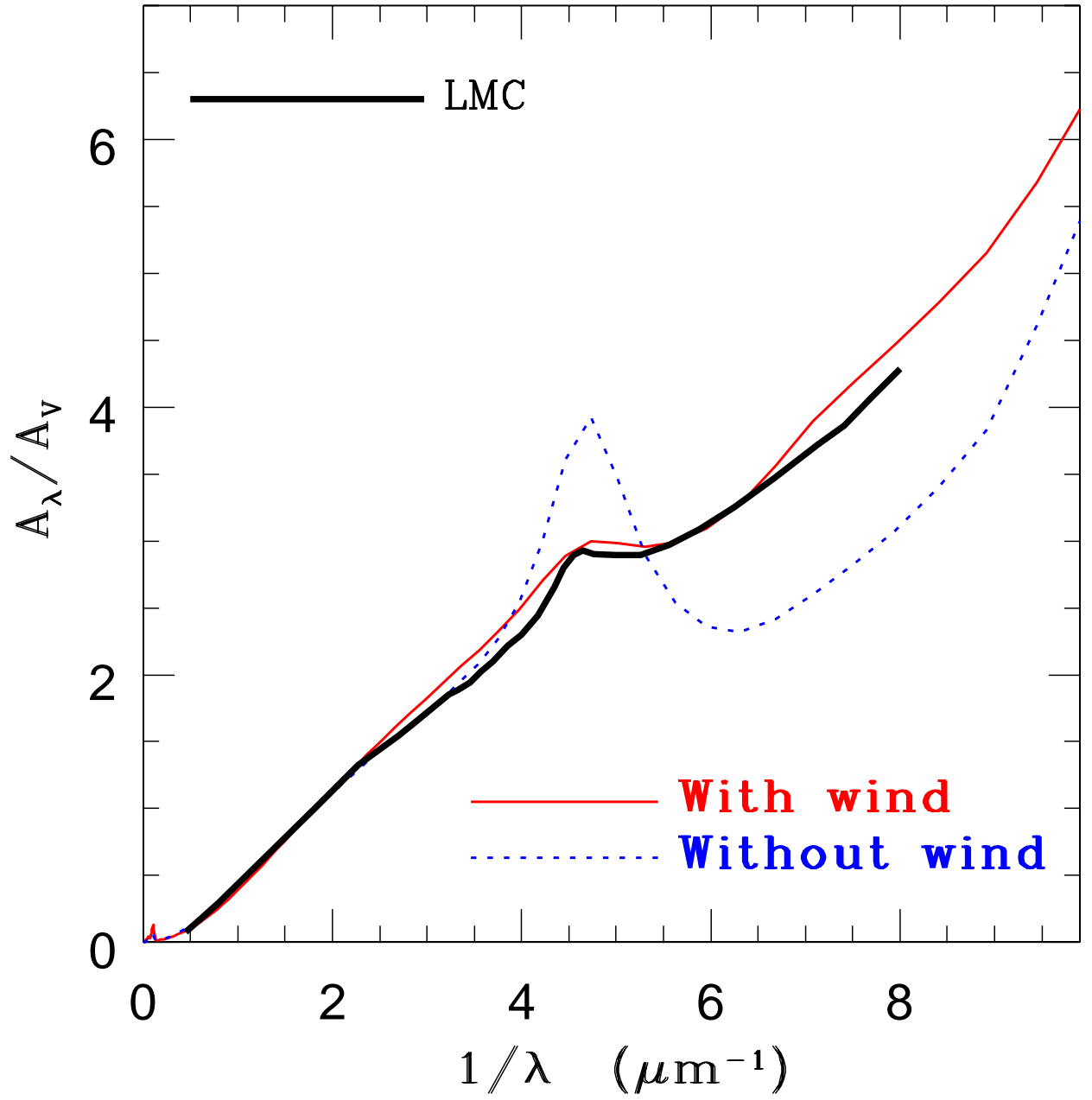


FIG. 7.— Extinction curves for the LMC models with dust wind (red solid) and without (blue dotted) at $T = 13$ Gyr (i.e, the present LMC). For comparison, the observed extinction curve is shown.

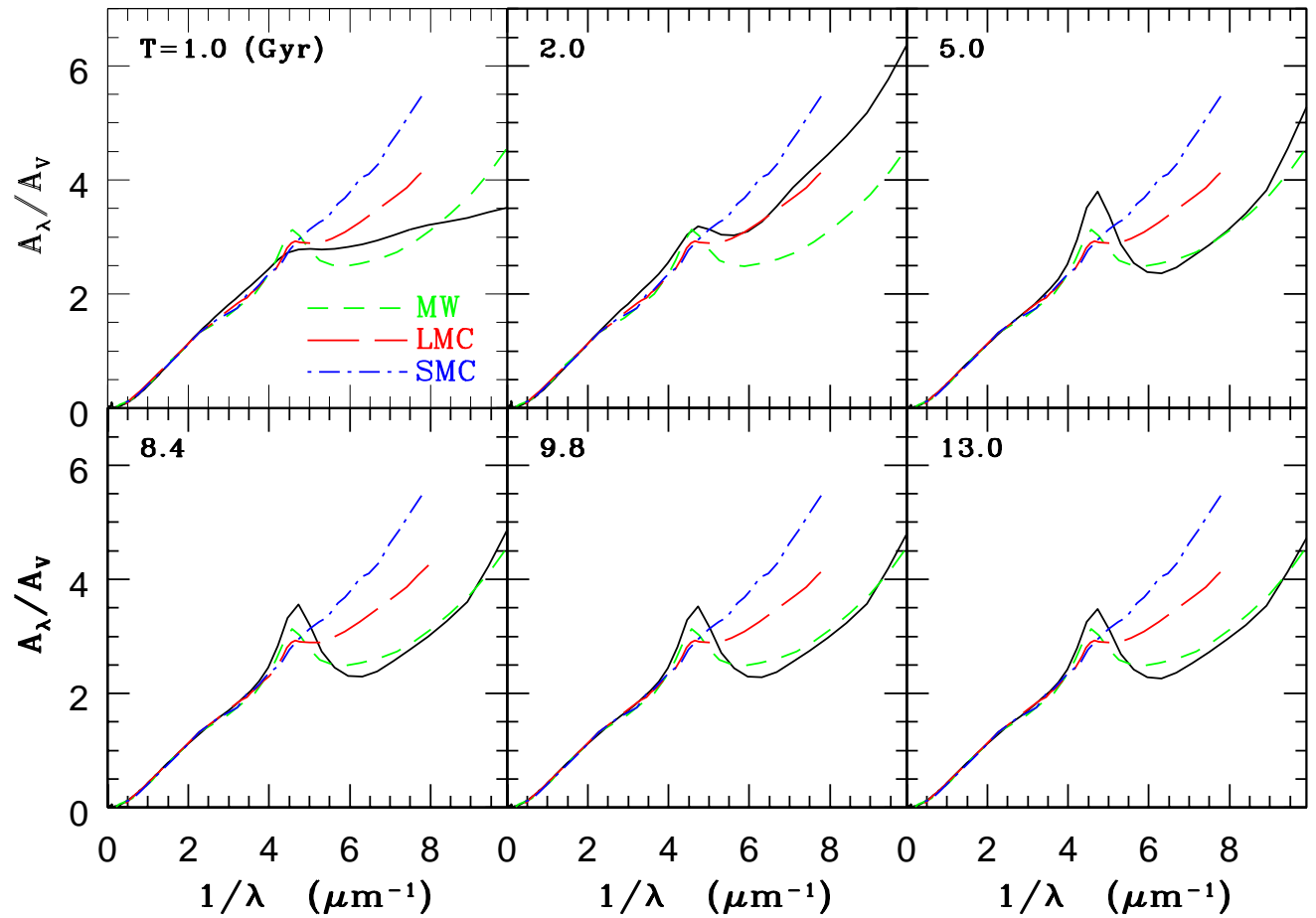


FIG. 8.— Same as Figure 2 but for the MW model M1 (without starburst and thus no dust wind).

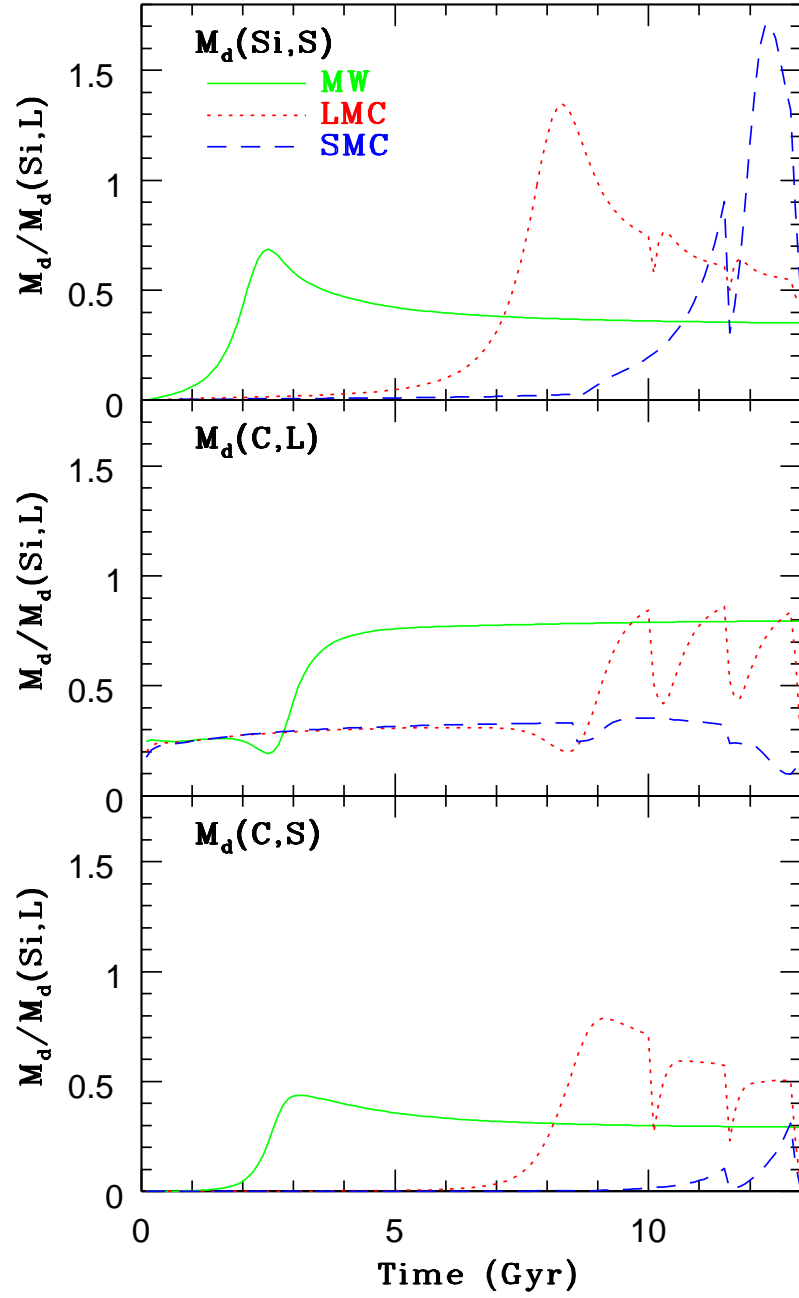


FIG. 9.— Time evolution of dust grain masses (normalized by the mass of large Si-grain, $M_d(\text{Si}, \text{L})$) for small Si-grain (top), large C-grain (middle), and small C-grain (bottom), for the MW M1 (green solid), the LMC L1 (red dotted), and the SMC S1 models (blue dashed).

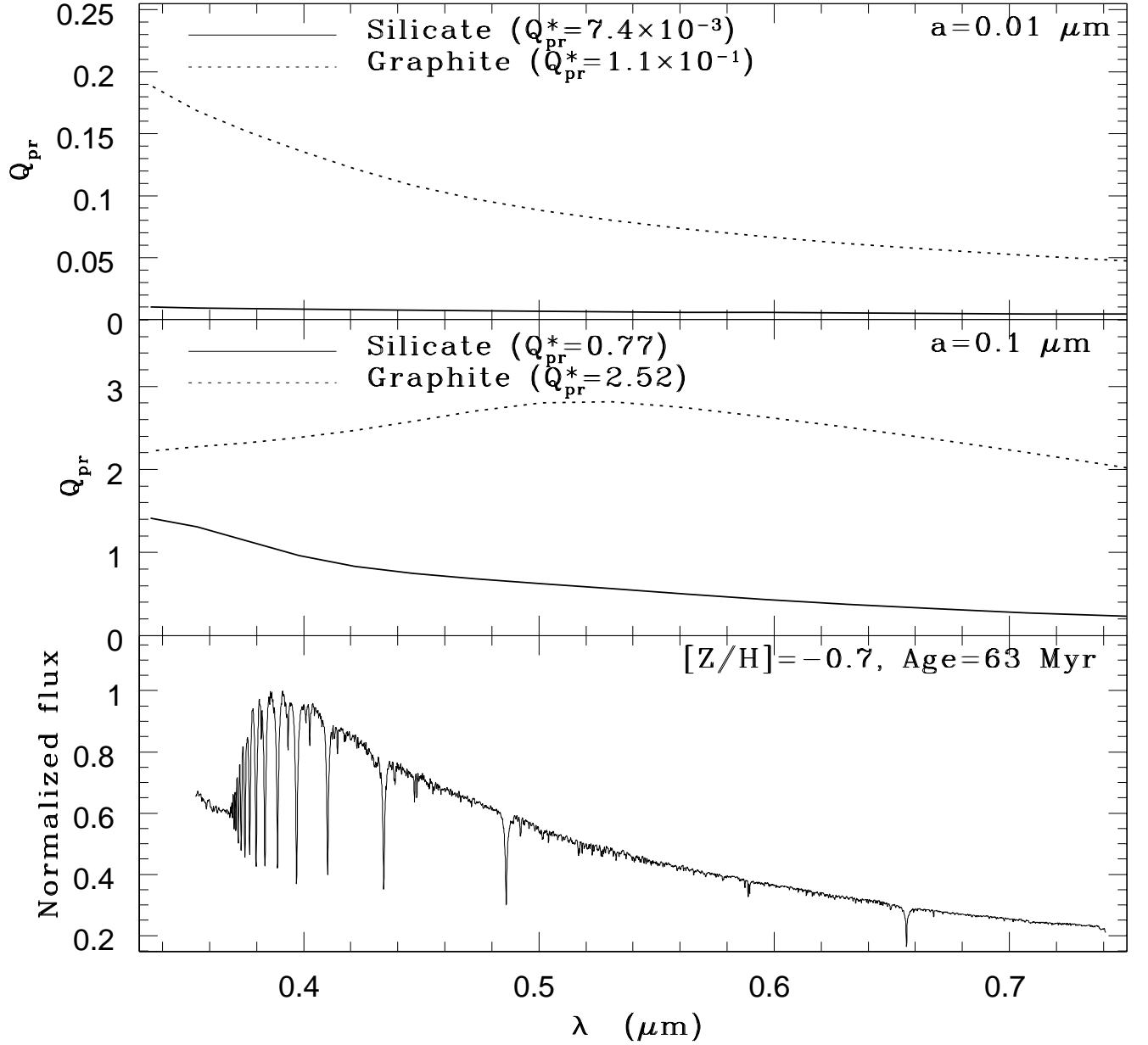


FIG. 10.— Dependence of the radiation pressure coefficient (Q_{pr}) for silicate (solid) and graphite (dotted) with dust radii (a) of $0.01 \mu\text{m}$ (top) and $0.1 \mu\text{m}$ (middle) on λ and the spectral energy distribution (SED) of a galaxy with $[Z/H] = -0.7$ and age of 63 Myr (bottom). This SED with the adopted metallicity and age can mimic the SMC with a recent enhanced star formation. The frequency-averaged Q_{pr} (Q_{pr}^*) for silicate and graphite are indicated in the upper part of the top and middle panels. Clearly, Q_{pr} is systematically larger in graphite than in silicate, which implies that graphite can be more strongly influenced by radiation-driven dust wind.

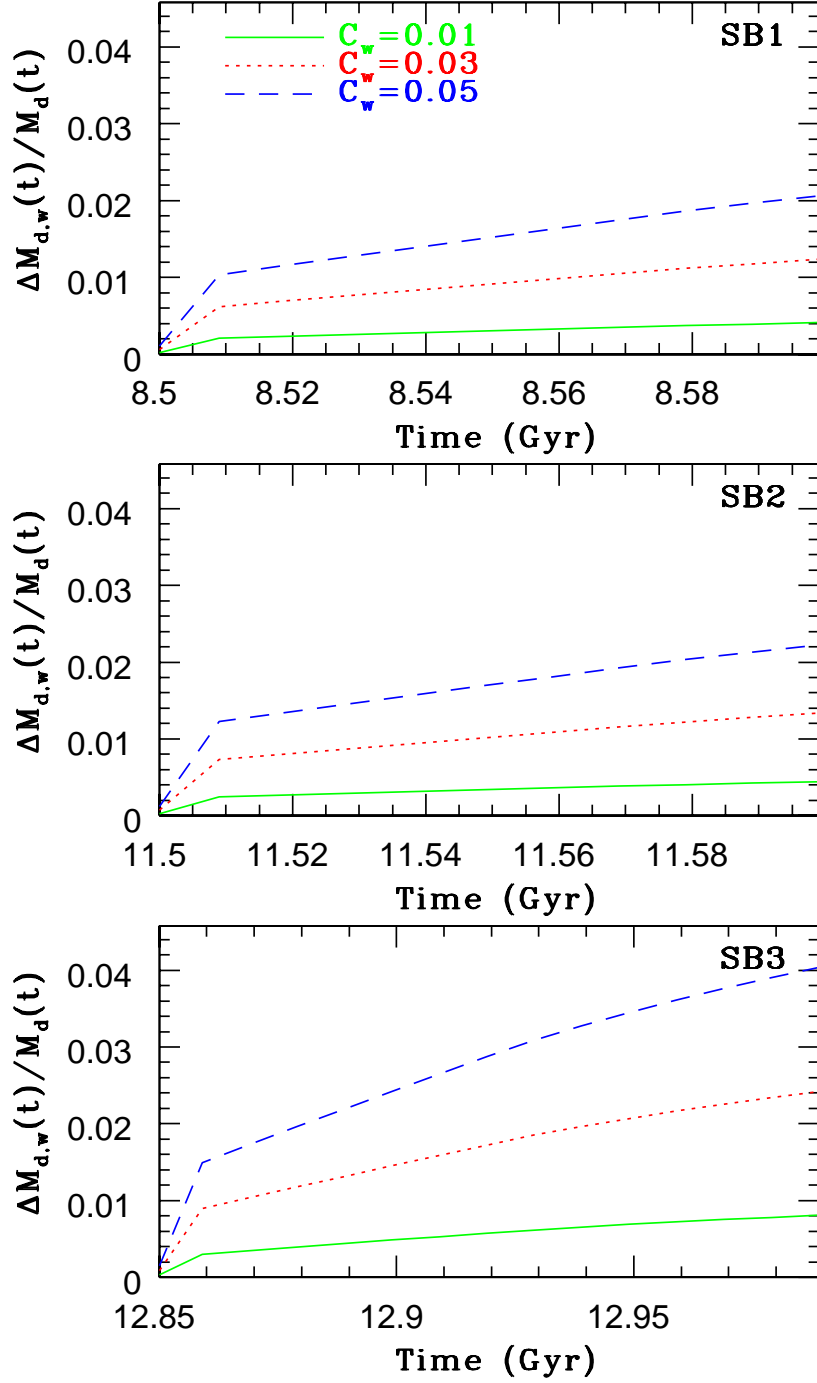


FIG. 11.— Time evolution of $\Delta M_{d,w}(t)/M_d(t)$ for the SMC models with $C_w = 0.01$ (green solid), $C_w = 0.03$ (red dotted), and $C_w = 0.05$ (blue dashed) in the three starburst epochs, SB1 (top), SB2 (middle), and SB3 (bottom). The same value for C_w (dust removal coefficient) is adopted for small and large silicate and carbonaceous grains (i.e., $C_{w,s,Si} = C_{w,l,Si} = C_{w,s,C} = C_{w,l,C} = C_w$) in these SMC models so that we can clearly demonstrate the physical meaning of C_w . The total mass of dust ejected from the SMC due to radiation-driven stellar wind ($\Delta M_{d,w}(t)$) is estimated at each time step and $\Delta M_{d,w}$ normalized to the total dust mass ($M_d(t)$) at the time step is shown in this figure. Given the time step width of 10^6 yr in the present study, $\Delta M_{d,w}(t)/M_d(t) = 0.01$ means that the SMC can lose 1% of its dust through dust wind in 10^6 yr.

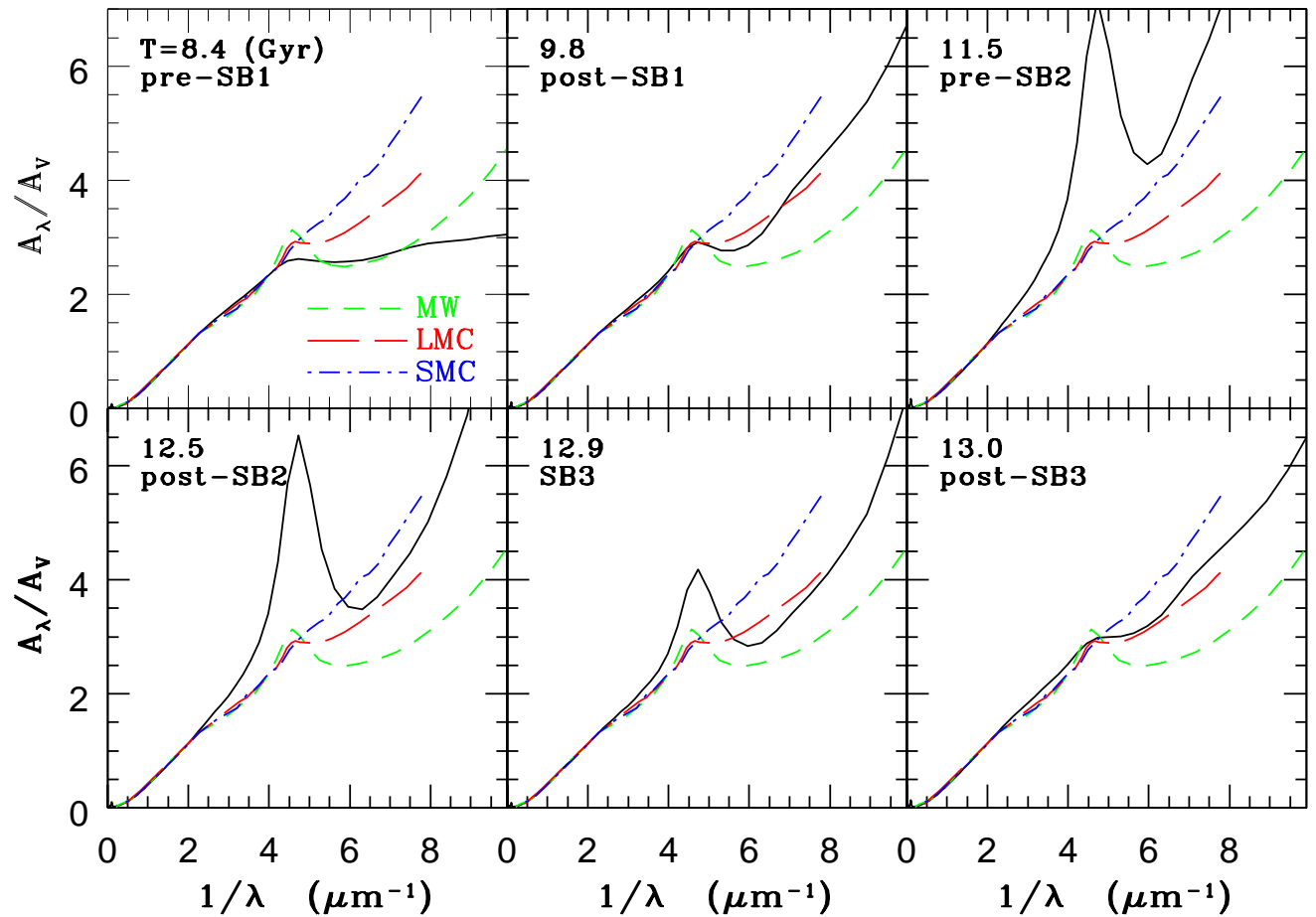


FIG. 12.— Same as Figure 2 but for the SMC model in which the strength of the first starburst (SB1) at $T = 8.5$ Gyr is twice as strong as SB1 in the fiducial model S1. In this model, other model parameters are exactly the same as those of S1.

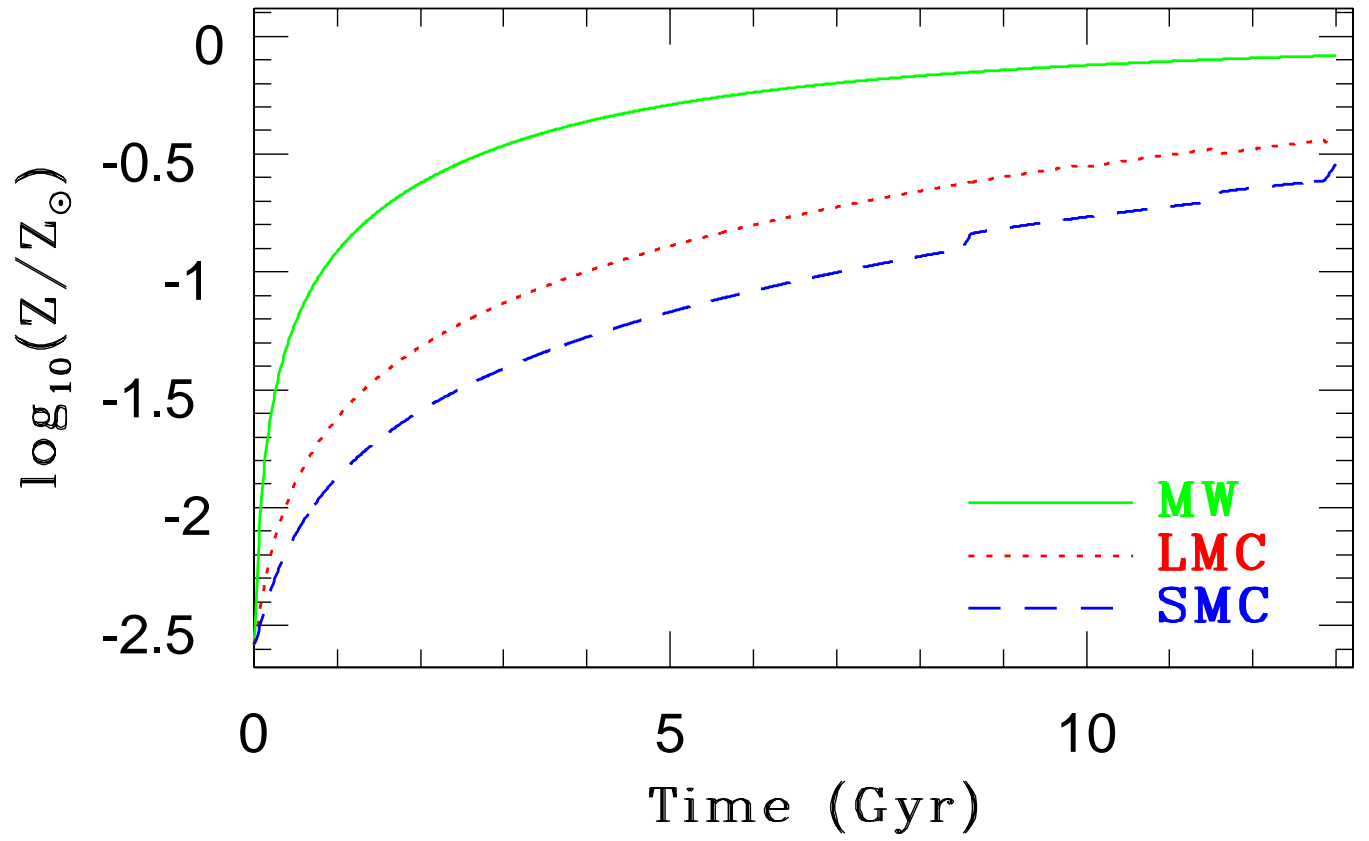


FIG. 13.— The time evolution of metallicities (Z normalized by the solar metallicity Z_{\odot}) for the standard MW (M1; green solid), LMC (L1; red dotted), and SMC (S1; blue dotted) models.

APPENDIX

THE PHYSICAL MEANING OF c_w

A key parameter for the time evolution of extinction curves of galaxies is C_w (dust removal coefficient) in the present study. Although an adopted value of C_w in a model can indicate whether dust can be removed more efficiently in the model than in other models with different C_w , the value of C_w (e.g., 0.01) itself does not represent the net rate of dust removal (e.g., $0.01M_\odot \text{ yr}^{-1}$) at each time step in the model. It is therefore important for the present study to relate C_w to the net rate of dust removal. Figure 11 shows the dust removal rate ($\Delta M_{d,w}(t)/M_d(t)$) at each time step in the three SMC models with different C_w . It is clear that (i) the dust removal rate is systematically higher for the model with larger C_w and (ii) it is higher in later starburst (i.e., higher in SB3 than in SB1).

The dust removal rate of 0.01 at a time step during a starburst in a model means that 1% of dust at the time step can be removed from the galaxy within the time step width of the model (10^6 yr). This furthermore means that during the starburst with the duration of 10^8 yr , the galaxy can lose $\sim 63\%$ ($= [1 - 0.99^{100}] \times 100\%$) of dust that it had before the starburst. The average $\Delta M_{d,w}(t)/M_d(t)$ is 0.0043, 0.013, and 0.022 for the three models with $C_w = 0.01, 0.03,$ and 0.05 , respectively. Therefore, $\Delta M_{d,w}(t)/M_d(t)$ (per Myr) can correspond roughly to $0.4C_w$ in the present study. It should be noted here that even for a constant C_w , $\Delta M_{d,w}(t)/M_d(t)$ of a galaxy can significantly change with time during a starburst owing to the rapid evolution of the total stellar luminosity of the galaxy during the starburst (See Figure 11). The normalized dust removal rate ($\Delta M_{d,w}(t)/M_d(t)$) might be useful for other theoretical models (e.g., one-zone models and numerical simulations with dust-related physical processes) that discuss the time evolution of dust in galaxies, particularly when they include radiation-driven dust wind.

DEPENDENCE ON THE STRENGTH OF STARBURST IN THE SMC

Although we consider that we have chosen a reasonable and realistic combination of C_{sb1} , C_{sb2} , and C_{sb3} for the SMC, it could be possible that the present results could depend on these three parameters. A particularly interesting question is whether the SMC can have an extinction curve without the 2175 \AA bump yet with the steep rise in the FUV regime in the early evolution phase if there is a stronger starburst. We have accordingly investigated the SMC models in which only C_{sb1} is different from the fiducial SMC model S1 so that we can address this issue. Figure 12 describes the time evolution of the extinction curve in the model with $C_{sb1} = 0.1$ (instead of 0.05 in the fiducial SMC model), which means that the first starburst is as strong as the third one in the model.

Clearly, the extinction curves in the early phase ($T \leq 9.8 \text{ Gyr}$) of this model are not so similar to the observed one of the present SMC, and this is true for the model even with $C_{sb1} = 0.2$. These results accordingly suggest that an extinction curve similar to that observed in the present SMC can not be achieved in the present models at early evolutionary phases by changing the strength of SB1 alone. These also imply that the SMC might have established its characteristic extinction curve quite recently. The final extinction curve in this model looks similar to the observed one for the SMC, but the degree of such similarity is higher in S1 than in this model, which means that the present fiducial model S1 chooses a more realistic parameter value than this model with $C_{sb1} = C_{sb3} = 0.1$ does. It is interesting that this model shows a more conspicuous 2175 \AA bump at $T = 11.5 \text{ Gyr}$ and 12.5 Gyr . It is confirmed that the observed SMC extinction curve can not be reproduced well in the SB2 phase of the SMC models with higher C_{sb2} ($=0.1$).

METALLICITY EVOLUTION

The time evolution of metallicities (Z) of the MCs and the Galaxy has been already investigated in detail by Tsujimoto & Bekki (2009), Tsujimoto et al. (2010), and BT12. However, the models adopted in these studies are different from the present one in the sense that they did not include dust-related physical processes (e.g., dust growth). Therefore, it is instructive for the present study to present the results of metallicity evolution in the new models. Figure 13 shows that the global trends of the metallicity evolution in the present three galaxy models (S1, L1, and M1) are very similar to those derived in our previous studies. However, the final metallicities at $T = 13 \text{ Gyr}$ are slightly smaller than the observed values of the galaxies: $Z = 0.0046, 0.0058,$ and 0.013 for S1, L1, and M1 models, respectively. These Z slightly smaller than the observed values are due largely to the more efficient loss of dust and metals through SN and dust winds in the present new models. The models with less efficient SN and dust winds can show higher Z that are closer to the observed values.